Tactile Sensory Responses in Motor Cortex and Their Relevance to Brain-Machine Interfaces

by

Karen E. Schroeder

A dissertation submitted in partial fulfillment
of the requirements for the degree of
Doctor of Philosophy
(Biomedical Engineering)
in The University of Michigan
2016

Doctoral Committee:

Assistant Professor Cynthia A. Chestek, Chair
Professor Joshua D. Berke
Assistant Professor Timothy M. Bruns
Associate Professor George A. Mashour
Assistant Professor William C. Stacey

DEDICATION

To my father, Dr. Brian Schroeder,

a celebrated teacher;

humble, contented, loving.

ACKNOWLEDGEMENTS

First and above all, I would like to thank Dr. Cindy Chestek. When I met you in 2012, I was immediately impressed with your knowledge, mentorship style, and productive, positive attitude. You have only increased in all these great qualities and more since that time. It has been my honor and privilege to work with you. You have handled every challenge with grace. You have shared so much with me, and been so generous with your time, thoughts and connections. Michigan is very lucky to have you.

A huge thanks to my committee. Dr. Tim Bruns, I have very much enjoyed observing and benefitting from your mentoring during your exciting start at Michigan. Dr. Bill Stacey, I have never had a conversation with you or observed you with a patient without learning something. Your advice to me before my qualifying exam motivated me to become a more confident, driven student. Dr. George Mashour, you have been a productivity juggernaut at the height of his game. I don't know how you do it all, but you do it with style. Your enthusiasm kept me going on many occasions. Dr. Joshua Berke, you are the finest teacher I have met. Though teaching may not be your favorite professorial activity, the time spent in your classes was the most rewarding time of my pre-candidacy. I regret that I could not repay all of your help and kindness over the years.

Thanks to my colleagues in the Chestek Lab: Zach Irwin, Kaile Bennett, Dave Thompson, Derek Tat, Nicole Bentley, Phil Vu, Autumn Bullard, Michael Kobylarek, Paras Patel, and Chrono Nu. I believe we have really experienced the full spectrum of human emotions in our time together. This humble collection of work can't properly represent how much we've grown, persevered, and triumphed these past few years. Thank you for all the memories. Zach, you have been the best possible labmate: patient, generous, talented, and charming. Kaile, you have been a great friend, my personal role model in multiple ways, and you made the lab feel like a family. Dave, you were an amazing teacher and friend.

Thanks to my mentors and colleagues from the Neural Engineering Lab – Matt Gibson, TK Kozai, Colin Stoetzner, Andre Snellings, Greg Gage, Amanda Perez, Rikki Hullinger, and Paras Patel – and to Dr. Daryl Kipke. I was nurtured by all of you into a competent student. Paras, I saved you for this section because we are NEL veterans together. We have been through a lot, but I have never been alone, knowing you were there for me. You have done uncountable favors for me; I hope I managed to give you a thing or two in return.

Thanks to my students in BME241 for a great teaching experience. You never failed to energize and impress me.

Thanks to my family, who have loved me unconditionally, most of all my mother. You have supported me in many ways, despite my insistence on trying to do everything myself. Completing this work without my father has been difficult, and at times, seemed pointless. Thank you for representing his approval as well as your own. You only ever supported my decisions, and told me to “enjoy the journey.”

Finally, thanks to my friends here in Michigan and from all over, who listened, supported, entertained, and inspired me. I feel so lucky to have had such a group of true, generous, intelligent, and trustworthy friends. Graduate school tested us in so many ways; I would not have made it out the other side without you. Each of you are so special to me, and I hope you know that. To Joe Labuz, Brandon Bruhn, Barry Belmont, Patrick Ingram, Yazan Billeh, Jayme Figueroa, Andrew Chong, Lynn Hurley, and Dan Wilson: I love you all.

TABLE OF CONTENTS

LIST OF FIGURES

LIST OF TABLES

ABSTRACT

The loss of hand function is a distressing and debilitating experience. Brain-machine interfaces (BMIs) hold the potential to restore natural movement to those with limb loss and paralysis by obtaining prosthetic control signals directly from the brain. Cortical BMI performance lags behind advances in prosthetic hardware, which may be due to lack of sensory feedback to the user and incomplete understanding of how motor cortex processes and uses sensory information. In this thesis, we explore tactile sensory representation in primary motor cortex (M1) and its relevance to the refinement of upper limb BMI with three independent but related studies.

The first study quantifies the frequency and robustness of tactile somatosensory responses within the same M1 cortical populations that are used for motor decoding. We show that M1 neurons are tuned to specific tactile fingertip inputs in both nonhuman primates and humans, and that units can be tuned differently to different sensory modalities. The modulation in firing rates is strong enough to interfere with motor decodes trained only on active motor tuning.

The second study investigates the source of this information stream, and its importance to sensory perception, using ketamine anesthesia. We show that corticocortical communication of tactile information between sensory cortex (S1) and M1 is interrupted during anesthetic-induced unconsciousness. When viewed along with the literature, the data suggest that M1/S1 communication is necessary for accurate conscious perception of sensory inputs, further reinforcing the need for sensory feedback in BMI experiments to enable naturalistic motor planning and execution.

The final study presents the design and testing of intracortical optogenetic stimulation devices for the further exploration of sensory processing, as well as the delivery of sensory feedback, by manipulation of specific neuronal subpopulations. We demonstrate that our implantable LED devices can safely drive neural activity in transgenic mice, and describe how they can be used to further refine closed-loop BMI.

Overall, we have advanced our understanding of M1 tactile sensory processing and developed stimulation devices for continued progress toward high performance neuroprosthetic systems.

Chapter 1

Introduction

> *"If I had a prosthesis that did what I want, then of course I would have been a full time prosthesis user."*
>
> *"I've broken a lot of things. I really have to watch what I do because…if I look the other way while lifting it, it will break."*
>
> - Upper limb prosthesis users describe their experiences. (Wijk and Carlsson, 2015)

We use our hands for hundreds of tasks each day: to communicate, to eat and drink, to groom ourselves, to interact with the world. The loss of hand function, then, can be a distressing and debilitating experience. Upper limb amputees experience greater frequency and severity of post-amputation pain, as well as more social and emotional issues related to their limb loss, than do lower limb amputees (Davidson et al., 2010). Over 500,000 people are living with upper-limb loss in the U.S. alone as of 2005, and this number is expected to more than double by 2050 (Ziegler-Graham et al., 2008). For these individuals, the tasks of everyday life present many challenges, even with the use of a prosthetic. Many amputees express dissatisfaction with the available options in prosthetic technology (Wijk and Carlsson, 2015), and current prosthetics available to the public (both body-powered and myoelectric) exhibit a high rejection rate. Even amongst consistent users of these devices, about 25% wear them simply for aesthetics and do not use any built-in functionality (Biddiss and Chau, 2007). In response to a 2002 questionnaire, 56% of amputees wore their prostheses "once in a while" or "never," and 64% rated them "fair" or "not acceptable" (Davidson, 2002). Underperforming prosthetics cause many amputees not to return to the workforce (40% of transradial amputees and 57% of proximal amputees) (Davidson, 2002), or return to a less demanding and lower-paying job, leading to a decrease in quality of life

as well as loss of income. Additionally, there are 1.3 million individuals with spinal cord injury in the U.S., over 140,000 of whom are tetraplegic (Spinal Cord Injury and Paralysis Research Center, 2009) and could benefit from brain-controlled prosthetics. There are currently no products for those with high level spinal cord injury to regain voluntary hand movements.

The roadblock to better prosthetic control is not the hardware – advanced, many degree-of-freedom prosthetic hands have been developed by a number of research institutions and private companies. It is the control signals to pilot these devices that need refinement (Andersen et al., 2014; Li, 2014). Signals obtained with currently available myoelectric controllers are simply not complete or precise enough to take advantage of the full complexity of hand movements, and typically are limited to a single grasp or pinching motion of varying quality. Some researchers are working on improving the signal quality of peripheral nerve implants, but ultimately the most effective solution is likely to be drawing signals directly from the source – the brain.

Brain-machine interfaces (BMIs) interpret brain activity to control external devices. Rich, finely tuned signals from individual neurons can be taken directly from the cortical motor output regions of the brain using intracortical microelectrode arrays and decoded into usable movement commands. Many years of research have gone into improving and optimizing the algorithms for this technique. Yet even as motor decoders become more sophisticated, a limiting factor in performance is the lack of sensory feedback to the brain. Patients with myoelectric prosthetics rely on visual and auditory feedback in order to properly grasp objects. When visual attention moves away from the hand or the line of sight is interrupted, control usually becomes impossible. This is frustrating to users, because the hand itself can obscure the object being held. In a survey of over 100 electrical upper limb prosthetics users, 45% rated sensory feedback as ‘absolutely important,’ with an additional 43% rating ‘medium importance,’ and more than half rated ‘grasping and holding’ most important, over touch and proprioception (Lewis et al., 2012). Patients in the clinical trials for intracortical BMIs experience the same difficulty – limitations in visual feedback make control very difficult (Wodlinger et al., 2015).

The following sections will discuss the connection between poor prosthetic control and the brain's need for accurate sensory information, and detail the gaps in knowledge addressed in this thesis.

1.1. Recent progress in upper limb prosthetic control

Over the past two decades, the BMI community has grown tremendously and reached some impressive milestones, including the first human clinical trials using chronically implanted intracortical electrodes. Substantial advances have been made in human cortical BMI over the past decade by multiple groups working with subjects with tetraplegia (Hochberg et al., 2006, 2012; Simeral et al., 2011; Collinger et al., 2013; Gilja et al., 2015; Jarosiewicz et al., 2015; Wodlinger et al., 2015). In these studies, subjects have been able to control an external prosthetic hand (in a laboratory setting) to feed themselves, shake hands, and interact with objects.

The advances in performance stem primarily from two concurrent efforts: first, to increase our understanding of how primary motor cortex (M1) naturally encodes movements, and second, to optimize decoding algorithms to maximize the amount of information that can be obtained from a limited subset of neural data. On the first point, it may surprise the reader to know that many of the bricks in our basic understanding of motor control are still missing or actively debated. Fortunately, BMI experiments in nonhuman primates (most commonly Rhesus macaque) have provided the perfect sandbox for the testing of M1 coding schemes (Hatsopoulos and Donoghue, 2009; Georgopoulos and Carpenter, 2015). Instead of analyzing individual cells' responses to movements offline, larger populations of neurons must be used to reconstruct movement parameters in real time. Shortcomings in our understanding of whole movement encoding immediately become clear under these conditions, demanding ever more comprehensive models.

One important enabler of upper limb BMI was the description of population coding of arm kinematics (Georgopoulos et al., 1986, 1988) – that an accurate estimate of reach direction could be drawn from a consensus of multiple individually tuned neurons. This was followed by a wave of closed-loop reaching experiments (Serruya et al., 2002; Taylor et al., 2002; Carmena et al., 2003) using M1 recordings, but there were still many open questions about the planning and generation of even a simple reach. The question of whether M1 encodes "intrinsic" (muscle

activity) or "extrinsic" (movement direction, limb position in space) variables has been long standing. Though decoders based on extrinsic variables have demonstrated impressive performance, they lack a mechanistic explanation. On the other hand, intrinsic models have recently been accumulating evidence. It is possible to predict myoelectric (EMG) signals in the arm using the activity of certain M1 units (Pohlmeyer et al., 2007; Ethier et al., 2012), and to generate realistic EMG from neural network models (Sussillo et al., 2015; DePasquale et al., 2016). But M1 correlates of both high and low level information have been abundant, and cells often unexpectedly change their coding schemes across behavioral contexts such as speed and posture (Scott, 2008), leaving the question very much an active area of exploration.

Another basic and enduring question for BMI control is the following: how much brain do we need to record from in order to control a complex, many degree-of-freedom arm? It is now known that M1 does not exhibit a highly segragated somatotopy (bodily map), as does primary somatosensory cortex (S1). Major bodily areas are segregated within M1, but smaller regions intermingle (Sanes and Donoghue, 2000; Sanes and Schieber, 2001; Schieber, 2001), with substantial overlap of, for example, muscles and joints of the hand and fingers. It's expected that an array placed in hand representation of primate M1 will produce a disorderly mixture of digit preferences. This is important to know for surgical implant logistics, but also points to the multifaceted response properties of M1 output cells. We know that M1 neurons exhibit both convergence and divergence: individual neurons diverge to innervate multiple muscles, and many M1 cells converge to innervate any given muscle. In keeping with this, several more recent studies have shown that both reaching and grasping can be decoded from the same (relatively) small population of cells on a single array (Carmena et al., 2003; Velliste et al., 2008; Vargas-Irwin et al., 2010). The latter study demonstrated that cells recorded from one 4 x 4 mm array could reconstruct 25 joint angles encompassing the hand, wrist and arm, and that individual cells often represented both proximal and distal joints. Human experiments have also achieved high dimensional control using only one or two 96-channel Utah arrays (Wodlinger et al., 2015). The authors believe that these data suggest M1 units encode quantities related to muscle activation, rather than explicit kinematics or kinetics of movements, and that M1 utilizes a distributed control scheme. This discovery is very encouraging for BMI, given that neuron counts (and the volume of tissue from an electrode array) are a limiting factor in decoding. We can likely do very

well with a limited number of arrays implanted in M1, if we have a system of sensory feedback in place, and continue working on the decoding algorithms.

1.1.1. Decoding algorithms

Neural firing rates can be decoded into motor commands by something as simple as a linear model, where the firing rate of a given neuron is linearly dependent on some set of kinematic movement parameters (hand position, velocity) (Georgopoulos et al., 1986). This technique is still sometimes used in human experiments (Wodlinger et al., 2015, for example) because it is relatively effective (at least in simple arm reaching paradigms), easy to train by patient observation of movements, and is not computationally intensive. However, there are other decoders that enable higher performance, a prominent option being the Kalman filter (Wu et al., 2006). The Kalman filter takes a Bayesian approach to the problem, incorporating prior information about neuron behavior and how kinematics evolve over time during a movement. This was shown to improve performance in monkey and human experiments (Kim et al., 2008; Simeral et al., 2011; Gilja et al., 2012).

At this point, it is pertinent to specifically draw attention to the fact that in the human BMI experiments, the decoders are typically trained by having participants observe actions, taking advantage of the fact that M1 neurons are responsive to this visual sensory stimulus and will 'mirror' the observed motor behavior. It becomes unclear how much of the decoded signal in subsequent online experiments is sensory, rather than a pure motor signal. In monkey experiments as well, proprioceptive signals are known to contribute to, or contaminate (depending on your outlook), motor decodes. This distinction might be unimportant were it not for the fact that the small population of recorded cells most likely has different tuning properties for different sensorimotor contexts, to say nothing of the differences in tuning between 'tasks,' such as an arm reach vs. grasping motion. And once experimenters begin providing tactile feedback, e.g. with intracortical microstimulation (ICMS) to S1, it will likely not be efficient to control a hand by both sending and receiving sensory information.

1.2. Somatosensory processing in the cortex

To begin to think about how to put sensory signals back into the brain, we need to understand the organization of natural somatosensory processing.

1.2.1. Somatosensory cortex

Somatosensory cortex (S1) of the primate is a mediolateral strip of cortex located just posterior to the central sulcus, across from M1 (Brodmann area 4). It is composed of Brodmann areas 3a, 3b, 1, and 2, moving anterior to posterior across the region (Qi et al., 2007). Area 3b is referred to as primary somatosensory cortex and is mainly concerned with sense of touch, having the most cells that respond to skin indentation, while 3a is concerned with proprioception, 1 with texture, and 2 with size and shape of objects (Krubitzer et al., 2004). Area 5 is not part of S1, but is known as association cortex, and has been shown to be involved with many kinds of sensory processing. Area 3b is highly somatotopic – most neurons in this area are responsive to touch on only a small region of skin. These areas are clustered by body part, which allows us to target most of the finger-specialized area of one hemisphere of the macaque with one 2 mm by 2 mm Utah array (Harvey et al., 2013).

S1 receives sensory information from multiple thalamic nuclei (Jones and Porter, 1980; Jones and Friedman, 1982). The pathways are fairly segregated, as shown in Figure 1.1.

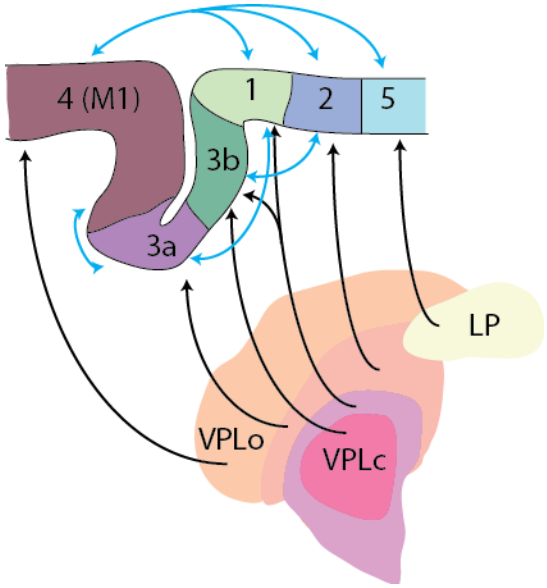

Figure 1.1 Thalamocortical and corticocortical flow of sensory information. VPLo: ventral posteriolateral nucleus (oral). VPLc: ventral posteriolateral nucleus (caudal). LP: lateral posterior nucleus. Adapted from (Jones and Porter, 1980) and (Jones and Friedman, 1982).

1.2.2. Primary motor cortex

M1 lies on the rostral bank of central sulcus. As mentioned earlier, it displays a generalized somatotopy for motor representation. It is much less appreciated, however, that M1 is also responsive to many kinds of sensory stimuli. An action like an arm reach-to-grasp requires the integration of visual, proprioceptive, and tactile information from multiple regions; for a detailed review of sensory integration for reaching, see (Sabes, 2011). Neuronal populations in M1 are sensitive to each of these types of sensory inputs. This has been shown in nonhuman primates (for an excellent and relatively recent review, see (Hatsopoulos and Suminski, 2011)) and to some extent in humans (Shaikhouni et al., 2013). Many cells are tuned to both sensory and motor

variables, though the tunings are not always directionally similar. Proprioception-tuned cells were found to be most tuned to the same or opposite direction as an active reach (Suminski et al., 2009). In studies on fast feedback control, corrective muscle responses occurring just 50-100 ms after a perturbation of the limb (Pruszynski et al., 2011, 2014), M1 neurons have been documented integrating arm joint information into corrective motor commands within 50 ms, reinforcing that M1 has significant and important sensory processing responsibilities.

M1 receives direct sensory inputs from deep muscle spindles via the ventral posteriolateral nucleus, oral portion (Figure 1.1, (Jones and Porter, 1980; Jones and Friedman, 1982)). Communication with S1 areas 3a, 1, 2, and 5 is necessary to access cutaneous information, and a substantial amount of 'deep' information comes via this route as well: stimulation of peripheral nerves elicits responses in M1, called 'evoked potentials,' which are reduced by 75% by ablation of S1 in the monkey (Asanuma et al., 1980).

1.3. Sensory feedback

Sensory inputs to M1 help to guide motor performance. Without them (or with only visual feedback, as is typically the case in BMI experiments), M1 is forced to adapt its control strategy. Multiple studies have shown that tuning of M1 cells is different during BMI control and natural movement (Taylor et al., 2002; Ganguly and Carmena, 2009), and that better performance can be achieved by allowing the ensemble to learn a new approach (Ganguly and Carmena, 2009; Orsborn and Carmena, 2013). While these measures have helped the situation, 'closing the loop' and delivering sensory signals to M1 will likely enable a large leap in performance, and will give users the sensation they desire.

1.3.1. Strategies for delivery of sensory feedback

How should we provide feedback to BMI systems? The capability to automatically sense and adjust prosthetic hand outputs is being developed (Edin et al., 2008; Roberts et al., 2011) using mechanosensors and optical sensors, but these methods do not give control to the users (users wish to handle a glass of water differently from a child's hand), and will not be useful at all for feedback of touch and proprioception. They also do not address the fact that M1 needs access to sensory inputs to generate correct commands.

The next option is electrical ICMS, which has been explored in rodents and primates, and works well enough in terms of supplying enough information to affect behavioral outputs. O'Doherty et al (2009) showed that monkeys could use ICMS as well as vibrotactile stimulation to inform the direction of an arm reach. Berg et al (2013) were able to transmit a percept of force applied to the finger with ICMS to S1. The problem is that ICMS does not integrate into closed-loop BMI well, because the electrical stimulus interferes with recordings in M1. The time intervals in which stimulation occurs must be removed, or 'blanked' from recordings (O'Doherty et al., 2012). This is a small amount of time (in the cited paper, 2-5 ms after each pulse), but enough to impact online control. Therefore, a different stimulus modality – light – is suggested to provide feedback similar in nature to ICMS but without the interference.

Optogenetics is a technique in which we use a viral vector to transfect a specific population of neurons with light-sensitive channels (Figure 1.2A). This allows us to stimulate these cells with

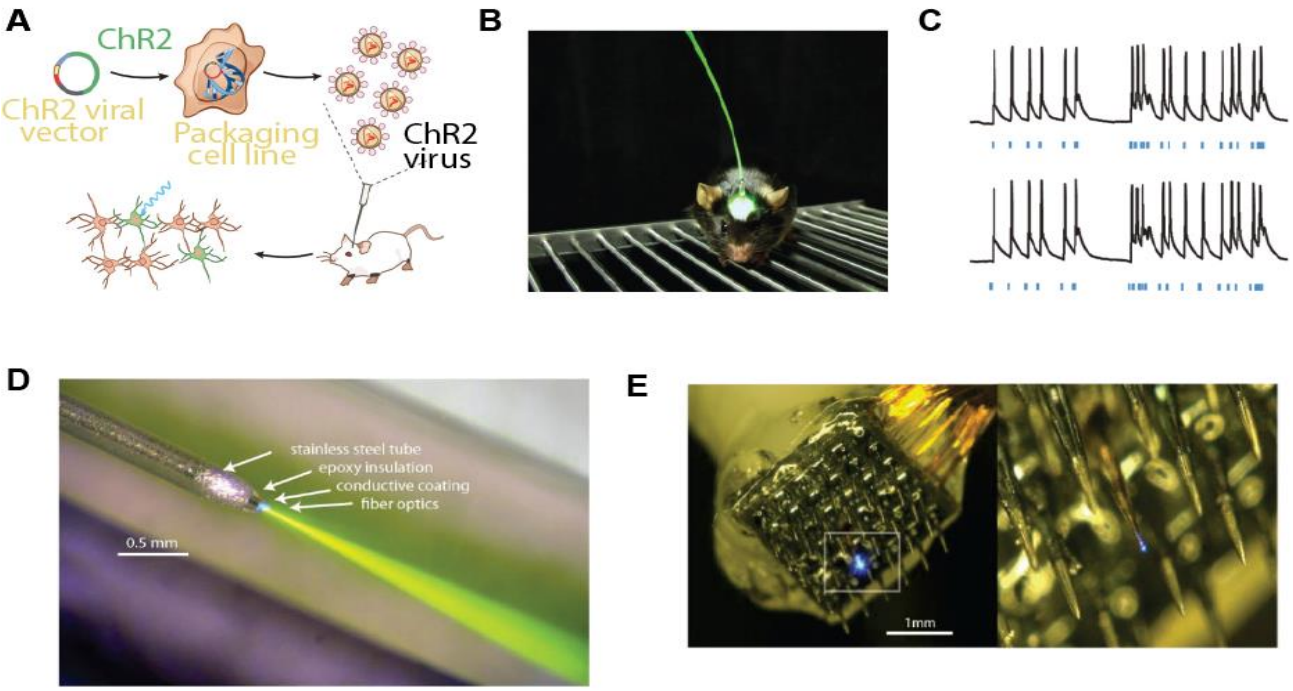

Figure 1.2 Overview of optogenetic techniques. (A) Method of creating light-sensitive cells: a viral vector (typically lentivirus or adeno-associated virus) is used to deliver a light-sensitive ion channel to the animal's brain. (B) Photograph of optogenetic mouse with laser-coupled fiber optic implant for light delivery. (C) Examples of light-driven action potentials. Blue dashes indicate laser pulses. (D) Laser-coupled fiber optic inside stainless steel guide tube for light delivery. (E) Laser waveguide integrated into Utah microelectrode array. (A-C) from (Diesseroth, 2015); (D-E) from (Wang et. al, 2011).

the application of light, instead of with electrical pulses that interfere with electrophysiology recordings. This technique has been widely adopted in the neuroscience community over the past decade thanks to its specificity – it is used to better understand neural circuitry by probing individual cells and pathways (Boyden et al., 2005; Zhang et al., 2007; review: Deisseroth, 2015). Since local populations of neurons can be precisely targeted (the spread of virus is limited around the injection site(s)), this technique is ideal for stimulating or inhibiting neurons to investigate sensory processing, or to provide multiple channels of sensory feedback in a BMI experiment. While the feasibility of translating this technology to humans is hotly debated, it remains a very useful technique in animal models.

Unfortunately, the currently available light delivery devices for primate experiments are single channel setups. Researchers use rigid glass optical fibers or microfabricated glass waveguides, either coupled to a recording electrode (Zhang et al., 2009; Wang et al., 2011, 2012; Abaya et al., 2012), or inserted separately (Jazayeri et al., 2012; Sparta et al., 2012; Ruiz et al., 2013). A high-power LED or laser is then coupled to the other end (Campagnola et al., 2008). In primates, this fiber must be inserted and removed for each recording session, limiting the number of total recording sessions based on tissue damage. It is possible to integrate fibers into a chronic Utah electrode array and let them remain in the brain for longer periods (Wang et al., 2012). Unfortunately, this has not been implemented successfully in primates without breaking the fibers or inflicting a large amount damage to the brain, due to larger motion of the brain inside the skull. An additional drawback of single-fiber implants in primates is the inability to excite or inhibit large volumes of brain, since light intensity drops off very quickly when passing through brain tissue. There is therefore a need for many-channel, chronically implantable light delivery devices for primate experiments. Such devices would greatly facilitate the development of sensory feedback strategies for upper limb BMI.

1.4. Summary of thesis

In this thesis, we explore tactile sensory representation in motor cortex and its relevance to the refinement of upper limb neuroprosthetics

In Chapter 2, we quantify the frequency and robustness of tactile somatosensory tuning within the same M1 cortical populations as are used for motor decoding. We show that M1 neurons are tuned to specific tactile inputs to the fingertips in both nonhuman primates and humans. The

modulation is strong enough to potentially interfere with motor decodes trained only on active motor tuning.

In Chapter 3, we study the source of this information stream and its importance to sensory perception using ketamine anesthesia. We show that corticocortical communication of tactile information between S1 and M1 is interrupted during anesthetic-induced unconsciousness. When viewed along with the literature, the data suggest that M1/S1 communication is necessary for accurate conscious perception of sensory inputs, further reinforcing the need for sensory feedback in BMI experiments to enable naturalistic motor planning and execution.

In Chapter 4, we develop and test intracortical optogenetic stimulation devices for the further exploration of sensory processing. We demonstrate that our implantable LED devices are functional in *in vivo* mouse experiments, in which we stimulated S1 while recording responsive units in M1. The ability to stimulate and record in different brain areas is a particularly useful achievement of this work, as this is precisely the setup that will be used for closed-loop BMI with tactile sensation.

In Chapter 5, we summarize the results and discuss future directions for this area of research.

Chapter 2

Quantification of tactile sensory finger representation in primary motor cortex of nonhuman primates and humans

2.1. Abstract

Challenges in the control of dexterous upper-limb brain-machine interfaces (BMIs) have prompted renewed interest in the amount and nature of sensory information encoded in primary motor cortex (M1). Previous single unit studies in monkeys showed M1 is responsive to tactile stimulation, as well as passive and active movement of the limbs. Recent work in this area has focused on proprioception, so here we examined how tactile somatosensation of the hand and fingers is represented in M1. We recorded multi- and single units and thresholded neural activity from macaque M1 while gently brushing individual finger pads at 2 Hz. Units displaying significant differences in firing rates between individual fingers ($p<.05$) represented 16.7% to 76.7% of sorted multiunits across four animals. After normalizing by the number of channels with significant motor finger responses, the percentage of electrodes with significant tactile responses was 74.9% ± 24.7%. No somatotopic organization of finger preference was obvious across cortex, but many units exhibited cosine-like tuning across multiple digits. Sufficient sensory information was present in M1 to correctly decode stimulus position from multiunit activity above chance levels in all animals, and also from electrocorticogram (ECoG) gamma power in two human subjects. Preliminary examination of unit tuning during tactile and proprioceptive inputs indicates cells are often tuned differently in different contexts, providing motivation for the refinement of BMI decoding approaches to dexterous grasping.

2.2. Introduction

Intracortical brain-machine interfaces (BMIs) hold the potential to restore natural movement to those with limb loss and paralysis by drawing prosthetic control signals directly from the brain.

Multiple research groups have enabled human subjects with tetraplegia to control an external prosthetic hand to feed themselves, shake hands, and interact with objects using signals obtained with microelectrode arrays (Hochberg et al. 2006; Simeral et al. 2011; Collinger et al. 2013; Gilja et al. 2015; Jarosiewicz et al. 2015; Wodlinger et al. 2015). Recently, there has been increased focus on the development of bidirectional interfaces to provide sensory signals back to users. It is likely that such feedback is necessary to enable high performance with many degree-of-freedom systems, particularly those involving dexterous manipulation of objects (Lebedev and Nicolelis 2006; Kwok 2013; Tabot et al. 2015). Intracortical microstimulation (ICMS) of primary somatosensory cortex (S1) cannot perfectly mimic a natural sensory percept, but it can provide a virtual tactile signal that monkeys can to use to complete BMI tasks (O'Doherty 2009; Berg et al. 2013).

With the development of these systems, it is important to consider the effects of sensory stimuli (both endogenous stimulation of the skin and virtual stimulation via ICMS) on M1 firing patterns used for motor control. Primary motor cortex (M1) itself is responsive to many types of sensory inputs, including proprioceptive, visual, and tactile (for a review, see (Hatsopoulos and Suminski 2011)). Many cells are tuned to both sensory and motor variables, though the tunings are not always directionally similar. M1 receives direct proprioceptive inputs from deep muscle spindles via the ventral posteriolateral nucleus (Jones and Porter 1980; Jones and Friedman 1982). Communication with cortical sensory areas 3a, 1, 2, and 5 is necessary to access cutaneous information, though a substantial amount of 'deep' information comes via this route as well: stimulation of peripheral nerves elicits responses in M1, called 'evoked potentials,' which are reduced 75% by ablation of S1 in the monkey (Asanuma et al. 1980). Though largely unexplored in more recent literature, specific examples of M1 cells responsive to tactile stimulation have been described in a number of single unit electrophysiology studies in monkeys (Lemon and Porter 1976; Wong et al. 1978; Lemon 1981; Tanji and Wise 1981). These studies found anywhere between 27-53% of units were responsive to cutaneous inputs, and the great majority of their receptive fields were on the glabrous skin of the hands and feet. Still, the extent, frequency, and tuning properties of these responses have not been fully documented, particularly in the context of array recordings, where the population of recordable units is more fixed.

Ignoring the importance of sensory signals in normal M1 firing patterns will likely become more of a problem as experiments incorporate more dexterous tasks. In human clinical trials, the presence of an object in or near the hand during an attempted grasp negatively affected decoder performance such that specialized calibration was required, and it could not be entirely corrected (Wodlinger et al. 2015). This and other BMI studies featuring interaction with objects (Velliste et al. 2008; Ethier et al. 2012; Hochberg et al. 2012) require a training set featuring objects to properly train the decoder. Wodlinger et al. note that without object training, the decoder will produce movements that repel the hand away from the object, instead of moving toward and grasping it. They suggest several explanations for this, one being expectations of tactile feedback. While unproven, this explanation would agree with the single unit data indicating the hands and feet have special M1 representation. It would also indicate robust sensory responses on those same motor electrodes, if the effects are strong enough to interfere with the decoder.

Another implication of M1 tactile responses is the possibility that they may cause overestimates in decoder performance during finger-related tasks. The most well-studied data sets for predicting our capability to decode finger movements online have come from mixed motor and sensory signals, as monkeys flexed their fingers to activate microswitches within a manupulandum (Ben Hamed et al. 2007; Aggarwal et al. 2008). These animals had constant tactile feedback as they performed the task, which would not be present in a patient using a clinical BMI system. Hand and finger decoding have also continued to improve in the ECoG BMI literature (Pistohl et al. 2012; Chestek et al. 2013; Hotson et al. 2016), but there is a persistent lack of clarity about the extent to which the decodes are relying on sensory versus motor signals.

In this study, we investigated the responses of M1 units to passive tactile and proprioceptive stimulation of the fingers of four macaque monkeys using intracortical microelectrode arrays. Although array recordings provide fewer isolatable units than can be achieved with repeated single unit insertions, their sensory content is of relevance to BMI performance. We found omnipresent M1 tactile fingertip representation, though the fraction of modulated units varied between animals. The tactile modulation was robust enough to successfully decode the sensory stimuli in these four animals, as well as in two humans with ECoG grids over M1. Many multiunits exhibited orderly tuning across the fingers that differed for the two types of stimuli.

The modulation in firing rates is potentially strong enough to interfere with motor decodes trained only on active motor tuning.

2.3. Methods

All animal procedures were carried out in accordance with protocols approved by IACUC at the University of Michigan. All human procedures were carried out in accordance with protocols approved by the IRB at the University of Michigan.

2.3.1. Surgery and experimental structure

Four rhesus macaques were implanted with multielectrode arrays in finger area of M1, as diagrammed in Figure 2.1A. Monkeys P and O were implanted with 2.5mm x 1.95mm 16-channel Floating Microelectrode Arrays (FMAs, Microprobes). Monkeys L and S were implanted with 4mm x 4mm 96-channel Utah Arrays (Blackrock Microsystems). Finger area was located by finding the point at which a line projecting from the genu of the arcuate sulcus would intersect central sulcus, and the arrays were placed as close to this point as possible, just anterior to the sulcus.

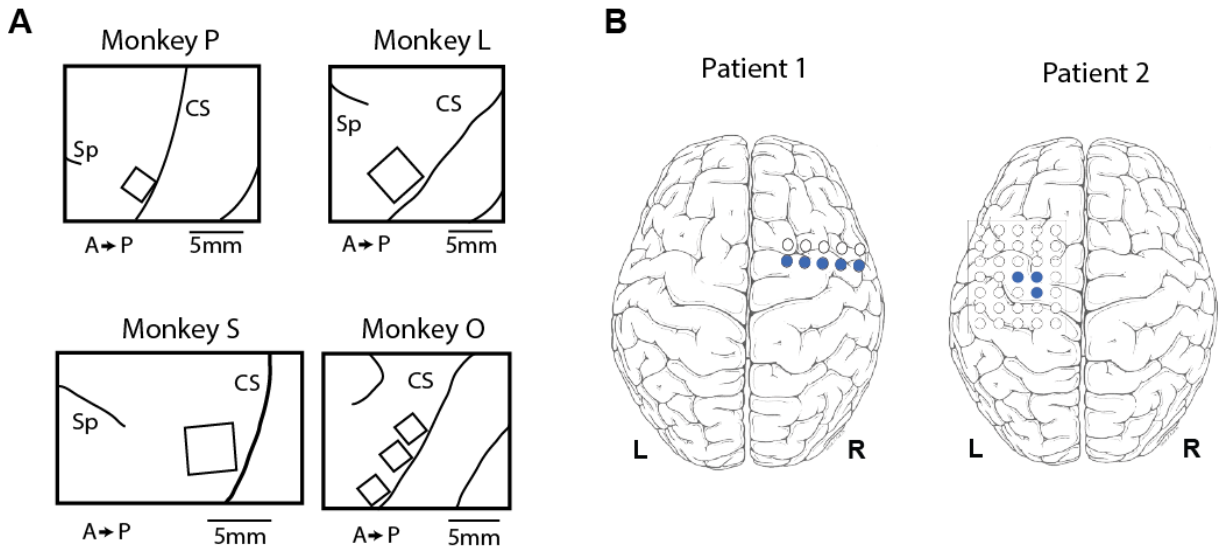

Figure 2.1 Placement of electrodes. (A) Array placement in four monkeys. Monkeys P and O had FMAs, while monkeys L and S had Utah arrays. CS: central sulcus; Sp: spur of the arcuate sulcus; A: anterior; P: posterior. (B) Subdural grid placement in two human patients. Blue circles indicate which electrodes were used in analysis.

We trained the monkeys over the course of several weeks to sit quietly in a chair (Crist Instruments) using small juice rewards. Animals' heads remained secured to the chair and motionless during all training and experiments with a titanium post (Crist Instruments) embedded in the head cap. For the brushing stimulus, the hand contralateral to the implant was immobilized against an acrylic plate, and a cotton-tipped applicator was used to stroke the appropriate finger pad at 2 Hz, as timed by a metronome. For the bending stimulus, the appropriate finger was grasped on each side and bent towards and away from the palm repeatedly for the duration of the trial.

All of the monkeys also performed an active motor task on different days from the sensory tasks. Monkeys S, L, and P performed a finger flexion task: each monkey sat in a shielded chamber with its hand resting on an acrylic surface, thumb pointing upward. The monkey was cued to flex and extend the four fingers to hit virtual targets with a virtual model of a monkey hand (Musculoskeletal Modeling Software; MDDF, Los Angeles, CA) displayed on a computer monitor. A resistive flex sensor (Spectra Symbol, West Valley City, UT) was attached to the index finger to measure finger position. Monkey O performed a grasping task: the monkey grasped a manipulandum instrumented with a pressure sensor (Interlink Electronics, Westlake Village, CA) located under the index finger pad and squeezed to hit virtual targets with up to 1 N of force.

2.3.2. Neural recording

A computer running xPC Target (Mathworks) cued the experimenter and synchronized behavioral and neural data for analysis. Trials were randomized and interspersed with rest trials, each lasting 5 seconds. The stimuli were entirely passive; if the monkey moved during any trial, it was flagged as invalid by an observing experimenter and not used in subsequent analysis. For monkey L experiments, the applicator was instrumented with a triple axis analog accelerometer (SparkFun) to better align behavioral and neural data.

Neural data were recorded at 30 ksps using a Cerebus neural signal processor (Blackrock Microsystems), high-pass filtered with a cutoff of 250 Hz, and sorted into single and multiunits offline using Plexon Offline Sorter (Fig. 2.2A). Only clusters that were completely separated in component space from the other waveforms on that channel, with blank space between, were considered to be single units. The remaining clusters, whether clearly containing multiple cells or

only slightly overlapping with other clusters, were combined to form up to one multiunit per electrode.

2.3.3. Human ECoG

Broadband neural data were recorded at 30 ksps from two human subjects who had been implanted with clinical subdural ECoG grids, as described in (Irwin et al., 2015). Grid placement is shown in Figure 2.1B. The same task structure was used as described in the previous section. The data were decimated to 10 ksps, and a common average reference was implemented for each bank. The data were then bandpass filtered between 66 and 114 Hz using a 3rd order Butterworth filter in MATLAB before calculating the power in that band during each trial.

A Naive Bayes decoder with leave-one-out cross-validation was used to classify the location of the stimulus on a given trial. The inputs to the decoder were the average band power on each included electrode during 2 seconds of stimulation. Chance level was 33.3% for a 1 of 3 choice, and the decoder could not perform better by choosing the most common condition, as the number of trials per finger condition were always balanced – between 20 and 24 trials per digit for the three datasets used (two from Patient 1, one from Patient 2). The two datasets from Patient 1

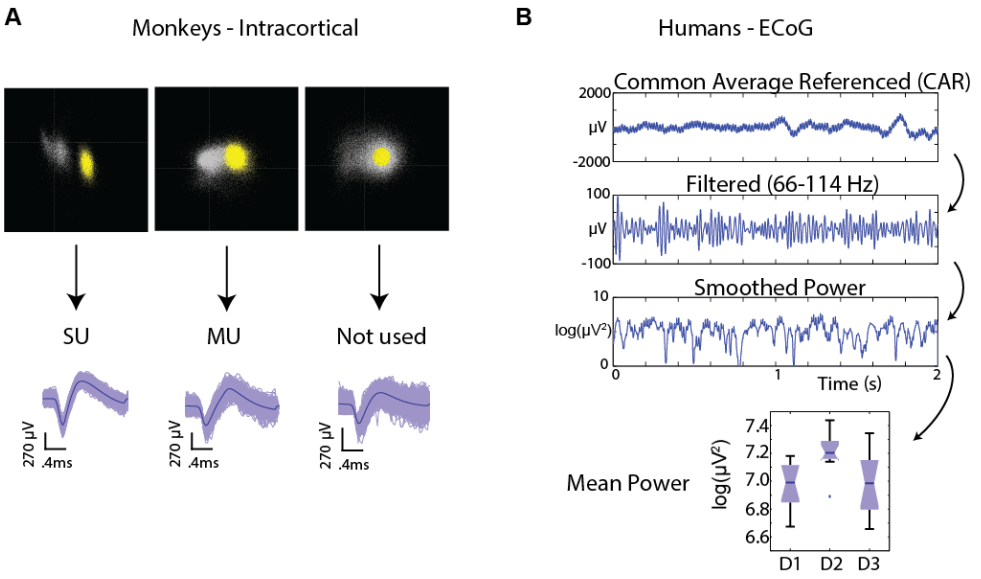

Figure 2.2 Processing of neural data. (A) Spikes were sorted in Plexon OFS into single units (SU) and multiunits (MU). (B) Human ECoG voltage data were common average referenced and filtered before being squared to obtain power. Mean power during three finger conditions were the feature set for the decoder.

were recorded on consecutive days. Electrodes were chosen by starting with the set of all electrodes that were entirely anterior to central sulcus on co-registration imaging. In Patient 1, a single row of electrodes over M1 was used, as seen in Figure 1B. In Patient 2, only a cluster over hand knob of M1 was used.

2.3.4. Spiking analysis and statistics

Significantly tuned units during the sensory brushing and bending tasks were determined with a one-way ANOVA, α=.05, of firing rates during trials of the different finger conditions. The total number of recorded units from each animal are the following: from monkey S, 73 multiunits and 68 single units from one recording; from monkey P, 27 multiunits and 12 single units from three recordings; from monkey L, 96 multiunits and 51 single units from two recordings; from monkey O, 15 multiunits and 12 single units from one recording.

Significantly tuned channels during the active motor task were determined by computing correlation coefficients between the finger speed (flex/extend task) or applied force (force task) and neural firing rates. In this case, spikes were detected by thresholding at -4.5 times the RMS voltage on each channel, after high-pass filtering the broadband signal at 250 Hz. Spike times were separated into 100 ms bins for each electrode. A null distribution was created by shuffling the firing rate bins and re-computing the correlation coefficients. Electrodes with coefficients at least two standard deviations above the mean of the null distribution were considered modulated by the motor task.

Tuning curves were fit to a Von Mises function (Amirikian and Georgopulos, 2000) in MATLAB, defined as:

$$f = b + m \exp[\kappa \cos(x - \mu)]$$

The parameter b represents the baseline firing rate, m the depth of modulation, κ the width, and μ the preferred 'direction,' or finger.

A Naive Bayes decoder with leave-one-out cross-validation was used to classify the location of the stimulus on a given trial, as in 2.3.3, except the inputs to the decoder were the firing rates of multiunits during the center 3 seconds of each trial. The beginning and end of each trial were excluded to avoid the periods of time when the experimenter was switching between fingers.

Chance level was 33.3% for a 1 of 3 choice, and the decoder could not perform better by choosing the most common condition, as the number of trials per finger condition were always balanced. Significance was determined with a 1-sample z-test with α=.01.

2.4. Results

We found units in each monkey that were visibly modulated by the tactile stimulus, as seen in the raster plots of multiunit spike trains sorted by 2 Hz content (Figure 3). M1 units with significant finger brushing modulation were found in all four animals tested (Fig. 4), though the fraction of units varied widely across animals, from 16.7% to 76.7% of sorted multiunits. Here, modulation indicates a significant difference in firing rates between finger conditions in the brushing task. Finger bending responses are also shown where available, for monkeys L, P and O. Passive finger bending is a proprioceptive stimulus that would be predicted to modulate some M1 neurons, though this fraction also varied widely. The difference in the number of modulated

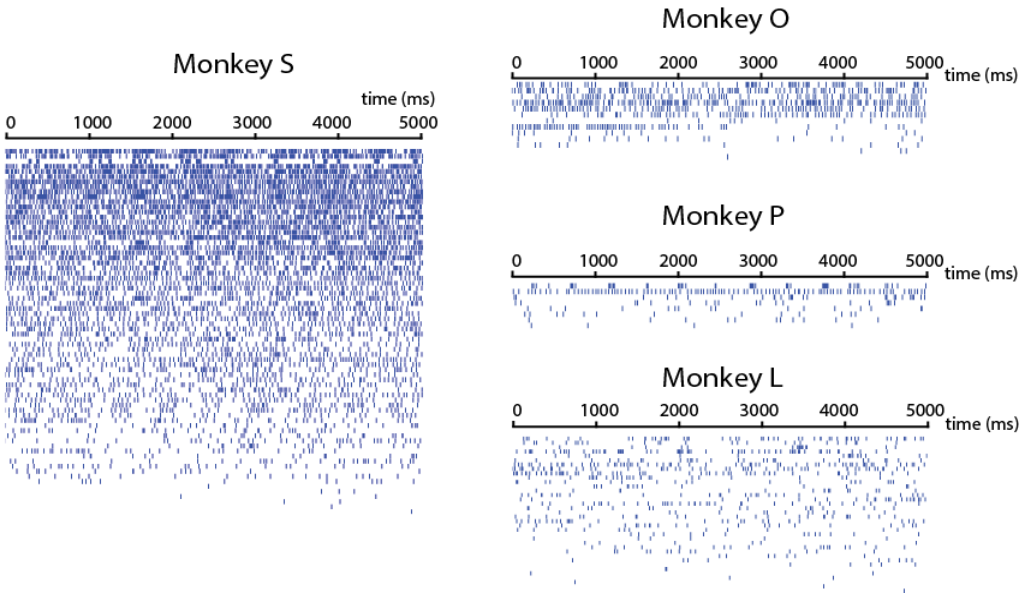

Figure 2.3 Example rasters from each monkey. For each monkey, all multiunits are shown for a single trial, sorted top to bottom by 2 Hz content.

units between monkeys can be attributed to some combination of poorer placement and inherent variance in sampling from a relatively low number of cells. To determine how well the arrays were placed in finger area, we examined the number of electrodes with significant modulation in a motor finger task that each monkey performed on a different day. Monkeys S, P, and L performed a finger flex/extend task, and monkey O performed a power grasp squeezing task. All

four monkeys had some amount of motor modulation, and the relative amount appeared to track with the sensory modulation, implying that a fair amount of the variance seen in sensory modulation was due to placement of the arrays. After normalizing by the fraction of electrodes with motor tuning, the percentage of electrodes modulated by the tactile stimulus was 74.9% ± 24.7%. The highest normalized fraction was seen in monkey P, who displayed, on average, an

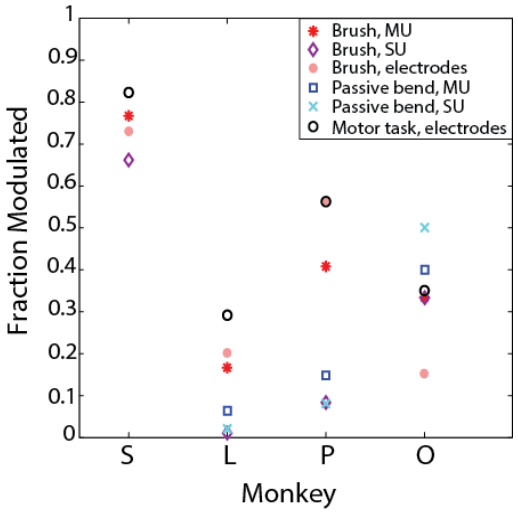

Figure 2.4 Fraction of recorded multiunits (MU) and single units (SU) that were significantly modulated by brushing and bending stimuli.

equal number of sensory and motor modulated electrodes.

No somatotopic or orderly organization of digit preferences was observed across cortex (Fig. 2.5), but rather an even scattering of multi and single units across the arrays. In monkey S, multiple single units were separable on certain electrodes, but only in some cases did those units share the same digit preference (Fig. 2.7). This result is consistent with our understanding of M1 somatotopy: large bodily areas are segregated, but representation of smaller features, like the digits, overlap significantly (Sanes and Donoghue, 2000; Sanes and Schieber, 2001; Schieber, 2001).

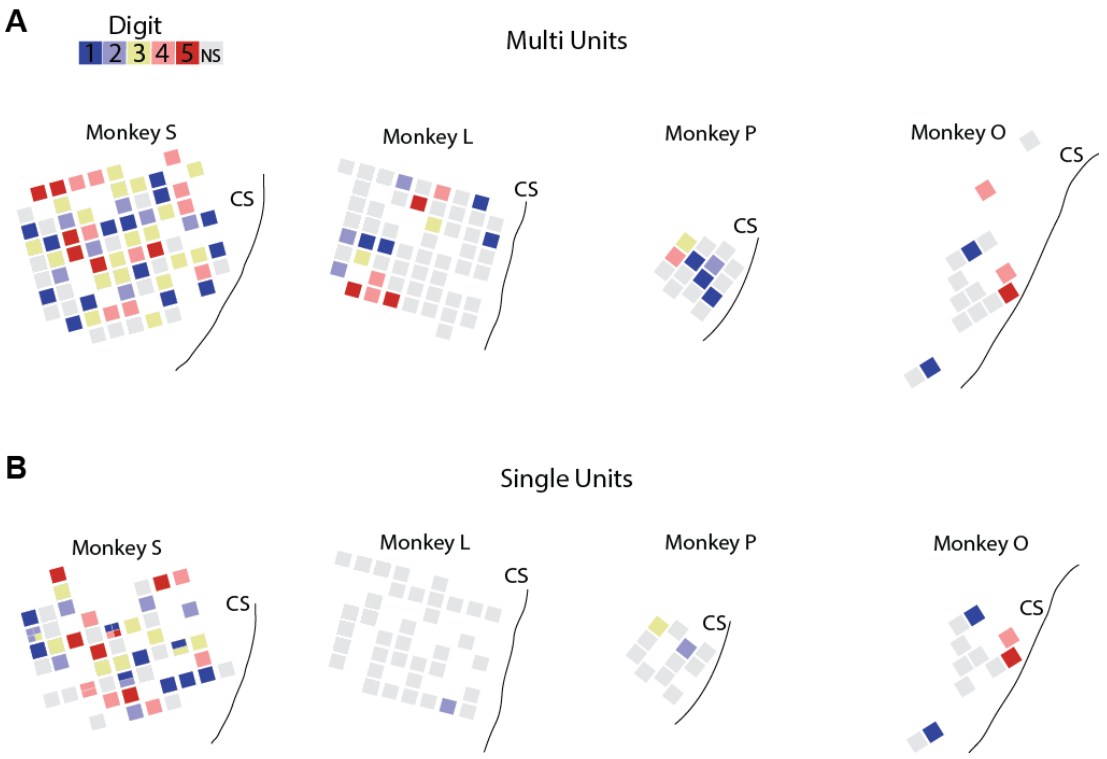

Figure 2.5 Distribution of digit preferences across electrode arrays. (A) Multiunit locations and (B) Single unit locations of modulated cells for brushing stimulus, colored by digit with maximum firing rate. Monkey S had several channels with multiple single units; preferences shown as divided squares. Grey squares represent units that were not significantly tuned. CS: central sulcus.

Investigating the receptive fields of these modulated units, we found that many of them were responsive to stimulation on multiple finger pads. Tuning curves for the single unit data (some example units shown in Fig. 2.6) exhibit different shapes, but shapely curves were seen far more often than linear slopes. As a comparison with directional tuning of motor cortical cells (Amirikian and Georgopulos, 2000), we fit the curves with a Von Mises cosine function. This function fit the data better than a linear or simple exponential for the majority of units, but there are only 5 digits on the hand, so it is most certainly overfitting the points. Still, the general shape of the fit is very good for the majority of units – R^2 was greater than 0.8 for over half of modulated units – indicating that these units generally have a receptive field that encompasses multiple adjacent finger pads with firing rates decreasing as the stimulus moves farther from the preferred digit.

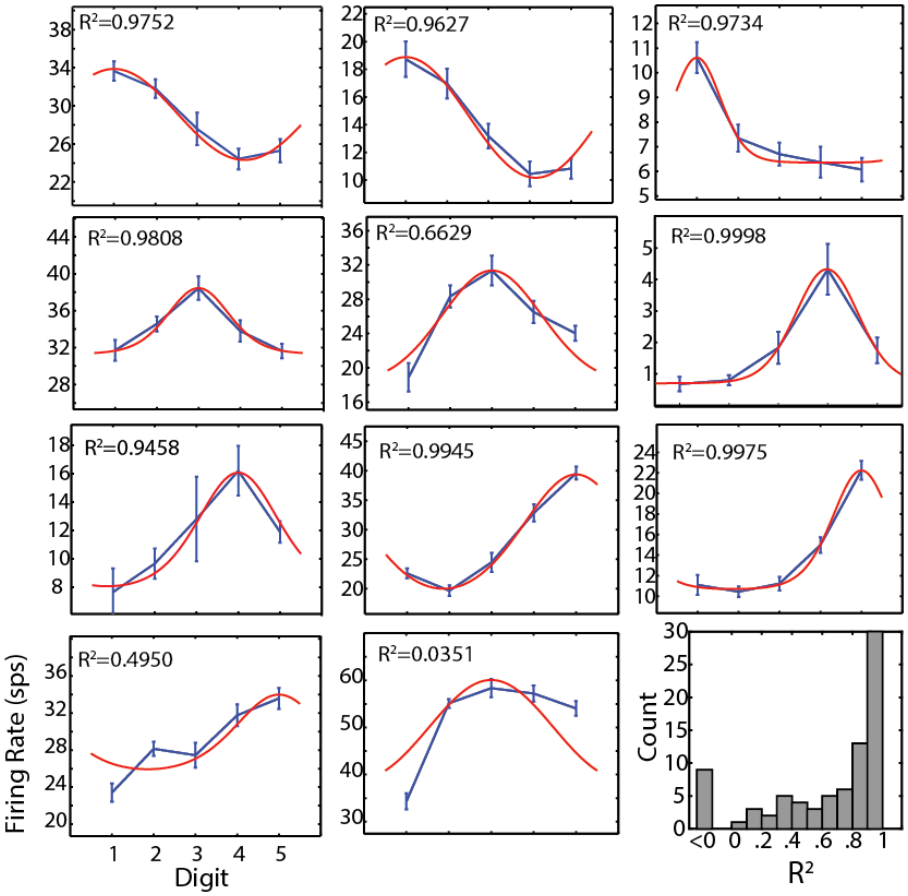

Figure 2.6 Tuning curves for brushing task. Example tuning curves showing the range of shapes observed in all four monkeys. Blue curves are data with linear interpolation; error bars show S.E.M. Red curves are Von Mises fits as described in Methods; R^2 shown for each panel. Bottom right: R^2 histogram for all modulated multiunits; value less than zero indicates a linear fit is better than the model.

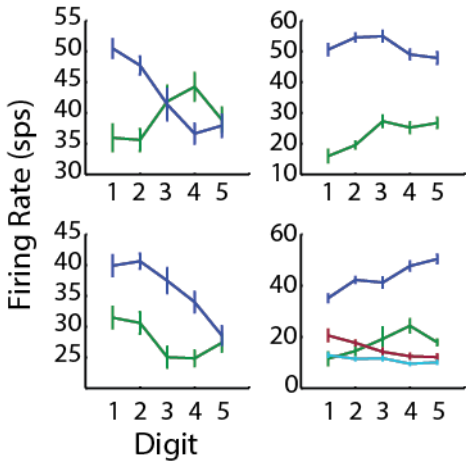

Figure 2.7 Tuning curves for multiple single units recorded on the same channel. All from monkey S.

Given the depth of tuning we found, along with the fairly even distribution of finger preferences, we were able to apply a Naïve Bayes decoder to classify the stimulated finger on a given trial based only on single or multiunit firing rates (Fig. 2.8). Multiunit decodes were significantly above chance levels (33.3% for a 1 of 3 choice, $p<.01$) in all animals. Single unit decodes were significant in two monkeys, but less reliable in monkeys L and P due to the very low number of modulated units available (visible in Fig. 2.5). Confusion matrices for Monkey O (Fig. 2.8A) demonstrate that digits 1, 4, and 5 were best represented, which agrees with recorded digit preferences (visible in Fig. 2.5).

We then applied the same Naïve Bayes decoder to gamma band (60-120 Hz) power recorded from subdural ECoG arrays in two human subjects. Above chance decodes were achieved in both subjects (Figure 2.9) using only M1 electrodes, and on two consecutive days in the first subject (P1 – 63.9% and 52.4% correct; P2 – 66.7% correct).

Monkeys P, L, and O underwent finger bending trials on the same day as brushing trials. We wanted to see if units were similarly tuned to both these sensory stimuli. Of those units that were significantly tuned in both conditions, only one shared the same finger preference during both (Figure 2.10). Though we had a small number of units, this data dovetails with previous work (Hatsopoulos and Suminski, 2011) showing that units in M1 are tuned differently to different types of stimuli.

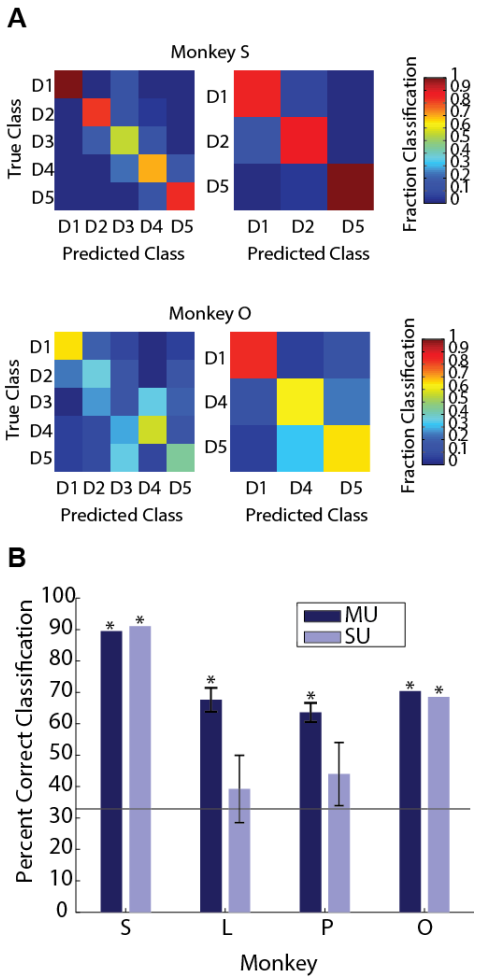

Figure 2.8 Decoding sensory stimulus from M1 firing rates. (A) Example 5 finger and 3 finger confusion matrices for monkeys S and O. (B) All 3 finger decoding performances for multiunits (MU) and single units (SU). Horizontal line indicates chance (33.3%). Asterisk (*) indicates significantly above chance ($p<.01$).

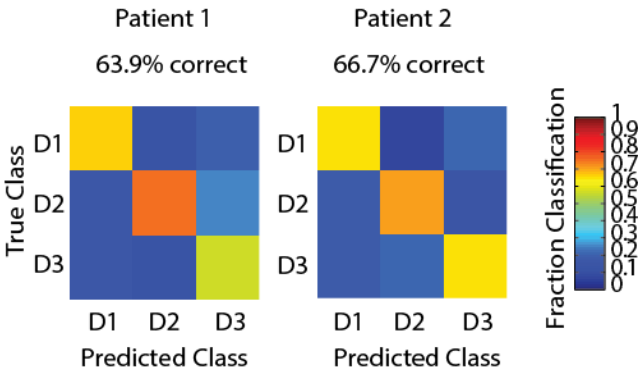

Figure 2.9 Decoding sensory stimulus from human gamma band power over M1. Patient 1 was also tested on a second day, with fairly similar performance (52.38%).

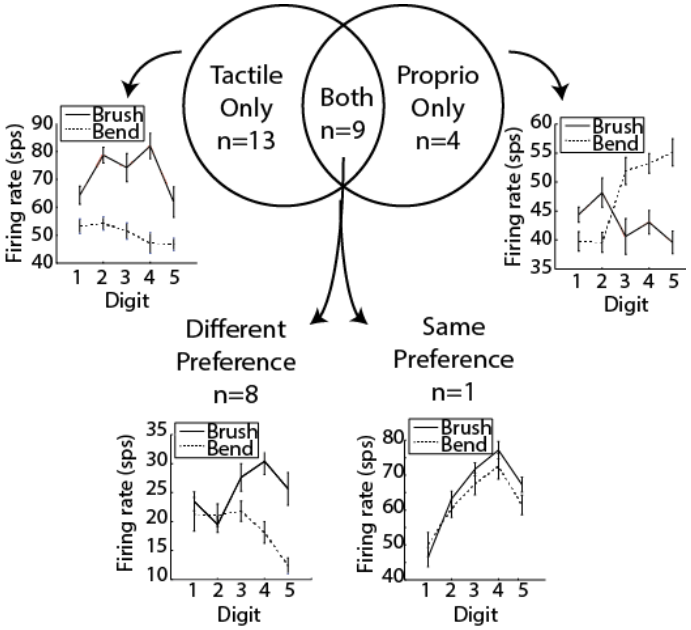

Figure 2.10 Comparison of tuning to tactile (brush) and proprioceptive (bend) stimuli. The Venn diagram shows the number of significantly tuned multiunits from monkeys P, L, and O when both types of stimuli were given in the same recording session. Examples of tuning curves for cases when units were tuned to the same and different digits are also shown.

2.5. Discussion

We have demonstrated that a substantial fraction of the M1 population is deeply tuned to tactile sensory inputs and readily apparent in multielectrode array recordings. The tuning was deep enough to correctly decode the location of a tactile stimulus from multiunit firing rates. While lower than previously reported finger motor decodes from M1 (Ben Hamed et al., 2007; Aggarwal et al., 2008, 2009; Egan et al., 2012), correct classification rates of 65-90% for a purely somatosensory stimulus were surprising, especially given the relatively low number of units recorded in monkeys P and O. This result provides evidence that motor finger decodes obtained previously are to some degree due to sensory responses. This result provides evidence for the possibility that motor finger decodes are to some degree due to sensory responses.

Similarly, the ECoG result demonstrates that sensory information is present in M1 recordings, in addition to the known motor responses in S1. In one ECoG study with successful individual finger decoding (Hotson et al., 2016), there was a large amount of overlap between channels used for motor (finger tapping) and sensory (vibrotactile) tasks, with the majority of electrodes

used being postcentral in both cases. The authors consider that the decoded "motor task" information may be mostly cutaneous and proprioceptive, or may also be to some extent an efference copy from motor areas.

This issue has probably not been a major factor in BMI decoding until recently because of the specificity of these responses to the hand and fingers. Tactile inputs are not as important to upper limb control as they are to fine motor control, evidenced by the specificity of representation to the hands and feet. Both rats and mice have a sensorimotor overlap zone (OL) where forelimb and hindlimb sensory and motor representations overlap (Donoghue and Wise, 1982; Tennant et al., 2011), and it is thought to be utilized for dexterous digit manipulation. While such a zone is not found in primates, it appears that M1 and S1 both engage in processing of sensory and motor information, and must therefore utilize corticocortical communication for dexterous tasks. There is ample evidence that M1 generates and sends sensory predictions that not only shape, but are in fact necessary for accurate sensory perception (Zagha et al., 2013; Manita et al., 2015; Morillon et al., 2015). Still, it is not possible to determine whether the responses recorded here represent M1 sampling or sending sensory information.

Given that the tactile M1 neurons we found also seem to be responsive to other types of stimuli (proprioceptive finger bending), and that proprioceptive-tuned cells in the literature can also encode motor outputs (Suminski et al., 2009), it seems likely that we are not recording a sensory-specific subpopulation. The changes in firing rates seen here were robust, and seem very capable of causing difficulty with motor decodes based purely on rate coding, in the cases where tunings differ. The multiunits such decoders are trained on are expected to have consistent preferred directions across all phases of the reach and grasp movements, when in reality, their preferences and functions change over time based on sensory context. The subject studied by Wodlinger et al. (2015) was able to grasp different kinds of objects, after having only trained on one kind, but still required an object-specific model. This was an important advance, but effective use of an arm in the real world will require many more types of grasps and movements in many contexts. Rather than viewing sensory responses as a troublesome contamination of motor signals, it's possible they could be harnessed to improve performance. Future work can develop strategies for training decoders in all of these contexts to best utilize the wealth of different tunings present on one electrode array. It's encouraging that with good placement, a single array is able to capture

representation of all the digits. Additionally, by studying the natural responses of M1 to tactile inputs, we can identify what information is important to provide when thinking about sensory feedback delivered to the cortex.

Overall, we have used chronically implanted microelectrode arrays to study the tactile sensory responses of a random sample of M1 neurons. This preliminary work motivates a more in-depth examination of population dynamics during fine dexterous tasks.

Chapter 3

Disruption of corticocortical information transfer during ketamine anesthesia in the primate brain

This chapter was published, as presented here, in the journal NeuroImage (*doi:10.1016/j.neuroimage.2016.04.039)*

3.1. Abstract

The neural mechanisms of anesthetic-induced unconsciousness have yet to be fully elucidated, in part because of the diverse molecular targets of anesthetic agents. We demonstrate, using intracortical recordings in macaque monkeys, that information transfer between structurally connected cortical regions is disrupted during ketamine anesthesia, despite preserved primary sensory representation. Furthermore, transfer entropy, an information-theoretic measure of directed connectivity, decreases significantly between neuronal units in the anesthetized state. This is the first direct demonstration of a general anesthetic disrupting corticocortical information transfer in the primate brain. Given past studies showing that more commonly used GABAergic drugs inhibit surrogate measures of cortical communication, this finding suggests the potential for a common network-level mechanism of anesthetic-induced unconsciousness.

3.2. Introduction

Most clinically-used general anesthetics act by potentiating the transmission of γ-aminobutyric acid (GABA), leading to depression of neuronal function and conscious processing (Alkire et al., 2008). Ketamine, however, does not depress the cortex and fails to conform to most mechanistic frameworks of general anesthesia: it does not bind with high affinity to the $GABA_A$ receptor (Antkowiak, 1999; Salmi et al., 2005), depress thalamic metabolism (Långsjö et al., 2005), activate the sleep-promoting ventrolateral preoptic nucleus (Lu et al., 2008), or depress high-frequency electroencephalographic activity (Lee et al., 2013). Identifying common neural features of ketamine and GABAergic anesthetics would therefore be an important step toward a foundational understanding of anesthetic-induced unconsciousness. We have recently

demonstrated in human surgical patients that ketamine, like the GABAergic drugs propofol and sevoflurane, depresses directed connectivity across frontal-parietal networks (Lee et al., 2013; Blain-Moraes et al., 2014). However, these and other electroencephalogram(EEG)- (Ferrarelli et al., 2010; Casali et al., 2013) and fMRI-based (Schrouff et al., 2011) connectivity studies of large-scale brain networks are based upon an assumption that the measured activity actually reflects information transfer along corticocortical pathways. A more direct measurement of functional connectivity of neurons and information integration is essential to validate these data.

In the current study, we used intracortical multi-electrode arrays in the *Macaque* brain to directly observe sensory information being shared between primary somatosensory cortex (S1, area 3b) and primary motor cortex (M1, area 4), two regions that communicate bidirectionally via local circuits through areas 1, 2 and 5 (Jones et al., 1978). We provided passive stimulation to the fingers of two monkeys (Fig. 3.1A), and recorded neural data from M1 and S1 before, during, and after ketamine-induced unconsciousness. We used a purely somatosensory, 2 Hz rhythmic stroking stimulation of the glabrous finger pads, which are quite sensitive to light touch. Along with S1, neurons in monkey M1 (particularly those in the most posterior region) are responsive to purely tactile stimulation of the digits, as well as passive movement (Fetz et al., 1980; Lemon, 1981; Tanji and Wise, 1981).

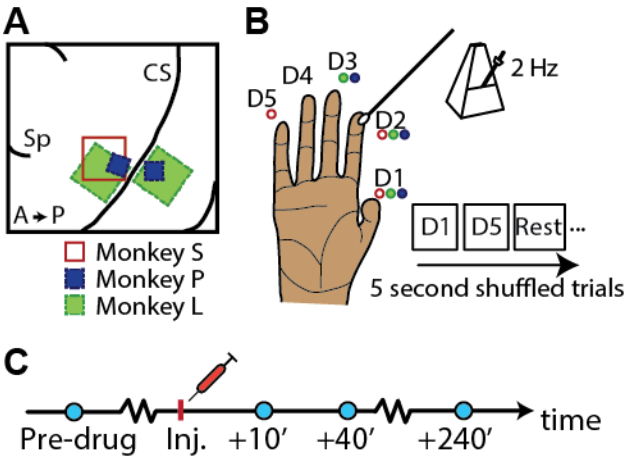

Figure 3.1 Electrode placement and experimental structure (A) Electrode placement in three monkeys. A: anterior; P: posterior; CS: central sulcus; Sp: spur of the arcuate. (B) Experimental trial structure and digits stimulated on each animal – color legend same as (A). (C) Trial block structure for each day of experiments. Blue marker denotes block of stimulation trials. Inj: intramuscular ketamine injection.

3.3. Methods

All procedures were carried out in accordance with protocols approved by the University Committee on Use and Care of Animals at the University of Michigan.

3.3.1. Surgery and experimental structure

Three rhesus macaques were implanted with multielectrode arrays in motor and sensory cortices,

as diagrammed in Figure 3.1A. In Monkey P, data was recorded from two 2.5mm x 1.95mm 16-channel Floating Microelectrode Arrays (FMAs, Microprobes), one of which was placed in finger area of M1, and the other placed in finger area of S1. In Monkey L, data was recorded from two 4mm x 4mm 96-channel Utah Arrays (Blackrock Microsystems), one of which was placed in finger area of M1, and the other placed in finger area of S1. In Monkey S, data were recorded from one 4mm x 4mm 96-channel Utah Array (Blackrock Microsystems) implanted in finger area of M1. The arrays were placed by first locating the point at which a line projecting from the genu of the arcuate sulcus would intersect central sulcus. The M1 array was placed at this location, just anterior to central sulcus. The S1 arrays were placed across from it, just posterior to central sulcus. Given the placement, size, and electrode length (1.5mm for Utah, 1.0-4.5mm for FMA) of the S1 arrays, a Rhesus atlas (Saleem and Logothetis, 2012) predicted that the majority of the recording sites would fall in Brodmann area 3b, although it is possible that a small minority, particularly in monkey P, were located in area 1.

We trained the three monkeys over the course of several weeks to sit quietly in a chair (Crist Instruments) using small juice rewards. Animals' heads remained secured to the chair and motionless during all training and experiments with a titanium post (Crist Instruments) embedded in the head cap. The hand contralateral to the implant was immobilized against an acrylic plate, and a cotton-tipped applicator was used to stroke the appropriate finger pad at 2 Hz, as timed by a metronome (Fig. 3.1B). Once monkeys were sufficiently trained, they each participated in 1 or 2 days of experiments with anesthesia. The time course of an experiment is shown in Figure 1C. Animals remained connected to the data acquisition system continuously for the first three time points to enable tracking of multiunits and oscillations over time. Monkey S is the exception to this, and only participated in an abbreviated experiment with two time points. At least two weeks were allowed between experiments for a given animal to minimize stress caused by side effects of anesthesia.

3.3.2. Neural recording

A computer running xPC Target (Mathworks) cued the experimenter and synchronized behavioral and neural data for analysis. Trials were randomized and interspersed with rest trials, each lasting 5 seconds. The stimuli were entirely passive; if the monkey moved during any trial, it was flagged as invalid by an observing experimenter and not used in subsequent analysis. For

monkey L experiments, the applicator was instrumented with a triple axis analog accelerometer (SparkFun) to better align behavioral and neural data.

Broadband neural data was sampled at 30 kHz and recorded using a Cerebus neural signal processor (NSP, Blackrock Microsystems). Collected data were processed and analyzed in three forms: 30 kHz broadband was saved and subsequently decomposed into frequency bands (see section 2.5), thresholded unit activity was obtained by thresholding at -4.5 times the RMS voltage on each channel, and multiunit activity was hand sorted using Plexon Offline Sorter. The data collected from each animal is summarized in Table I.

TABLE I

SUMMARY OF COLLECTED DATA

	Monkey L	Monkey P	Monkey S
# Experiments	2	2	1*
Implant(s)	M1+S1, Utah	M1+ S1, FMA	M1 Utah
# Electrodes M1/S1	64/64**	16/16	96/0
# Multiunits M1/S1	94/37	17/18	50/0
# Trials per time point	48-66	30-65	40-75

*Only pre-drug and +:10 time points collected; **Only 64 channels from each array were recorded simultaneously

3.3.3. Anesthesia

Ketamine was administered once per experiment as a 10 mg/kg intramuscular injection to the upper thigh while the animal was seated in a chair. Arousal was monitored at least every 15 minutes until the animal was fully responsive, particularly before each set of experimental trials. The metrics of arousal used were vertical nystagmus, pedal (toe pinch) reflex, blink reflex, limb manipulation (picking up arm or leg and allowing to fall into experimenter's hand), and spontaneous movements. Although ketamine levels in the blood were not monitored, anesthetic effects seen at each time point were common to all animals, and are described in Table II. Due to the one-time administration of the drug, the level of anesthesia was not identical at the different time points; indeed, we wished to investigate features of the neural signal at these different points.

TABLE II

OBSERVATIONS OF ANESTHETIC DEPTH

Test	+10 Minutes	+40 Minutes	+240 Minutes
Spontaneous movement	None	Occasional facial or hand movement	Normal movement of limbs, face and torso
Pedal reflex	No movement	Minimal response, if any; some digit flexion	Strong withdrawal
Blink reflex	No movement	Occasional weak blinking	Normal blinking
Limb manipulation	No response when handled	Minimal response; some digit flexion	Limb withdrawn when handled
Vertical nystagmus	Present	Present	Not present

3.3.4. Data analysis - Spikes

A Naive Bayes decoder with leave-one-out cross-validation was used to classify the location of the stimulus on a given trial. The inputs to the decoder were the firing rates of either thresholded activity or hand sorted multiunits during the center 3 seconds of each trial. The beginning and end of each trial were excluded to avoid the periods of time when the experimenter was switching between fingers. Only three fingers per animal were used in order to increase the number of trials completed per finger, given the time restraints of the anesthesia. The particular fingers used for each monkey were chosen during a separate session of awake stimulation. The fingers with the greatest number of channels responsive to stimulation, as compared with a rest condition, were used for subsequent experiments. Only modulated thresholded channels or multiunits were used; modulation was determined with an ANOVA (α=.05) of firing rates during the different finger conditions. Chance level was 33.3% for a 1 of 3 choice, and the decoder could not perform better by choosing the most common condition, as the number of trials per finger condition were always balanced. Percent correct at each time point was tested for significance versus chance with a one-sided one-sample z-test. The number of datasets used for decoding from each brain area were 5 for M1 (3 animals) and 4 for S1 (2 animals).

The power spectrum for each multiunit was computed using the center 3 seconds of each trial,

split into 1 ms bins. These binned spike trains were then converted to a spike density function (SDF) by convolution with a Gaussian kernel (σ=15 ms). The power spectra of the SDFs were then computed with Matlab's discrete Fourier transform, *fft*. The spectra of all units for all trials were then averaged together and normalized by the peak power, which occurred between 0 and 1 Hz. Data for this analysis were taken from two monkeys (P and L), who each completed two experiments.

High order transfer entropy (HOTE) was computed using the Transfer Entropy Toolbox for Matlab (Ito et al., 2011). Data for this analysis were taken from two monkeys (P and L), who each completed two experiments. Data were prepared by taking multiunit sorted spike trains, extracting spike times during the center 3 seconds of each trial (the same portions as used for decoding), and concatenating them to form one vector per multiunit per experiment with length between 3 and 6 minutes. Equal numbers of awake and ketamine trials were used for each experiment. Spikes were then binned in 1ms bins and passed to the toolbox, which calculated HOTE for each possible multiunit pair. All entropies were 5th order, with possible time lags of 1 to 30 ms. Only the peak, or maximum, value for each multiunit pair over all possible time lags was included in plots. For shuffled HOTE, S1 spike trains were shuffled using Matlab's *randperm* before calculating peak HOTE for each pair.

3.3.5. Data Analysis – Oscillations

The recording sessions from monkeys L and P were split into 5 second bins where the signal was free from high amplitude artifacts, and then power spectra were created for each bin using MATLAB's *fft* function. Power at 1Hz increments (1-4 Hz for delta, 13-30 Hz for beta, and 40-80 Hz with 59-61 Hz excluded for gamma) were calculated and then averaged together in 1 minute increments over 100 minutes of the experiment. Power on all electrodes were averaged together, smoothed with a window size of 10, and normalized by dividing by average power over the entire 1-80Hz band. Example spectrograms (Fig. 3.5B) represent single electrode activity from a single experiment with monkey L. The Chronux toolbox for Matlab was used to generate the spectrogram plots after data were decimated and bandpass filtered between 0 and 80 Hz.

3.4. Results

3.4.1. Loss of sensory information transfer during ketamine exposure

Before ketamine administration, the identity of the stimulated finger could be correctly classified from thresholded neural activity on the M1 and S1 electrodes (Fig. 3.2A) using a Naïve Bayes decoder, with a mean accuracy of 68.7% from M1 electrodes and 89.3% from S1 electrodes. After an intramuscular injection of ketamine (10 mg/kg), animals reached unconsciousness within 10 minutes, as judged by lack of pedal and eye blink reflexes. From 10 to 30 minutes post-injection, while animals were completely unresponsive, decoding performance from M1 decreased to chance levels (Fig. 3.2A), with a mean of 27.4% correct. The consistency of the stimulus in monkey L was verified with stimulator-mounted accelerometers; no difference in the number of strokes before or after ketamine were found on either day (p=.67/p=.26, t-test). At 4 hours post-injection, when consciousness had returned, M1 decodes recovered to 54.4% correct, significantly above chance. Importantly, even when M1 decodes were disrupted, S1 decodes did not significantly decrease. This result is consistent with the hypothesis that, during exposure to ketamine, sensory information can still reach S1 from the thalamus, but is prevented from reaching M1 via an interruptible corticocortical pathway. It should be noted that surrogates of preserved primary sensory processing, such as somatosensory-evoked potentials and intra-network connectivity of primary sensory cortex, have been observed during unconsciousness induced by

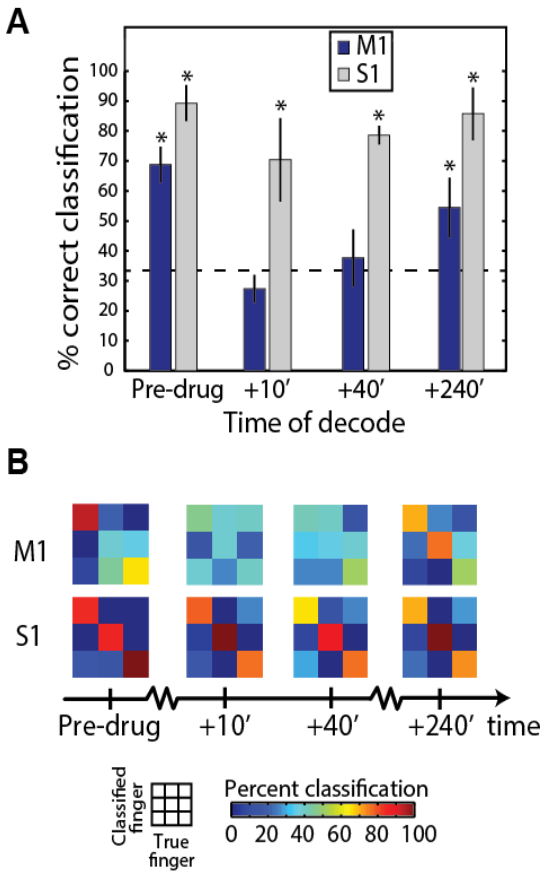

Figure 3.2 Loss of sensory representation from motor cortex under ketamine. (A) Percent correct classification of stimulated finger across all monkeys and sessions. *p<.001 when compared to chance level (dashed line). Error bars denote S.E.M. (B) Example confusion matrices showing decoder performance for one session of Monkey P.

GABAergic anesthetics in humans (Banoub et al., 2003; Boveroux et al., 2010).

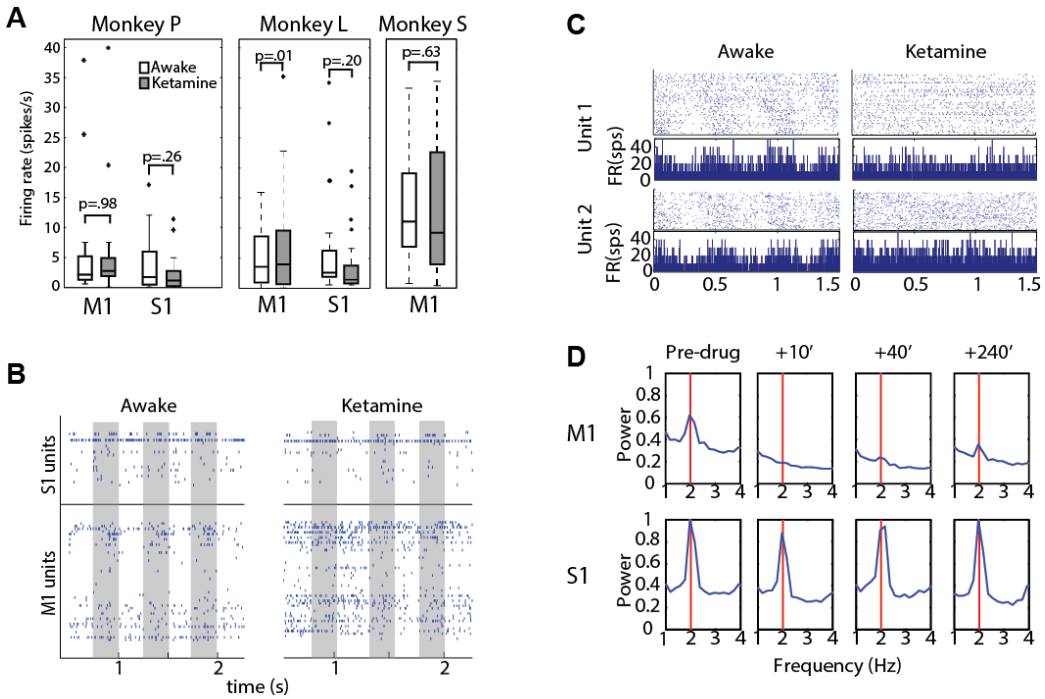

Figure 3.3 Multiunit behavior and power spectra. (A) Firing rates of sorted multiunits before and after ketamine (+10' time point). (B) Example raster plot of all recorded multiunits during portions of one awake trial and one ketamine trial from monkey L. Grey bars: stimulator in contact with digit. (C) PSTHs of two example M1 units, aligned to first stimulus of trial. (D) Normalized mean power spectra for unit activity averaged across modulated units from monkeys P and L. Red vertical line emphasizes 2Hz, the frequency of stimulation.

In addition to ensemble representation, the behavior of hand-sorted multiunits was analyzed (see Methods). Decodes performed with multiunits followed the same pattern as thresholded data, with a mean percent correct classification of 52.5% correct from M1 and 74.84% correct from S1 while awake, decreasing to 26.12% (chance level) and 68.69% respectively at 10 minutes post-injection, and finishing at 49.15% and 76.28% after 4 hours. Lower percentages than those achieved with thresholded data were expected, considering the small number of well-isolated units compared with the number of unsortable channels with clear bipolar activity. Mean firing rates remained stable among M1 and S1 multiunits (Fig. 3.3A): while some cells increased and others decreased their firing rate, paired t-tests revealed no significant changes in overall firing rates in any animal, after correcting for multiple tests. Examples of unit responses are shown in Fig. 3.3 B and C, with stimulus-aligned bursting activity shown for several M1 units. The

presence of a 2 Hz peak (the frequency of stimulation) in the power spectra of M1 and S1 single unit spike trains (Fig. 3.3D) followed the pattern of decoding performance, disappearing in M1 units under ketamine anesthesia and recovering at the final time point. The magnitudes of the peaks from pre-normalized S1 unit spectra did not change significantly (paired t-test, α=.05) from pre-drug to 10 minutes post-injection.

3.4.2. Loss of functional connectivity during ketamine exposure

Knowing that M1 and S1 have reciprocal, though not necessarily monosynaptic, corticocortical connections (Jones et al., 1978), we investigated whether the disappearance of M1 representation could be explained by a loss of functional connectivity between the two regions. We applied high order transfer entropy (HOTE), an information-theoretic measure of directed connectivity between neurons (Ito et al., 2011), to multiunit spike trains from monkeys L and P. HOTEs were computed for each possible multiunit pair during a given recording session. Inter-region connectivity decreased significantly for combined monkey sessions (Fig. 3.4B) as well as for each individual session (all paired t-tests, α=.05, n=1,889 total M1/S1 pairs). These results support the observation of reduced information transfer between the two cortical regions under ketamine. Intra-areal S1 HOTE also decreased, which was not necessarily expected, given its sustained sensory representation. This reflects a decrease in the ability of S1 neurons to help predict each other's behavior in general, which may indicate a larger change in S1 firing behavior

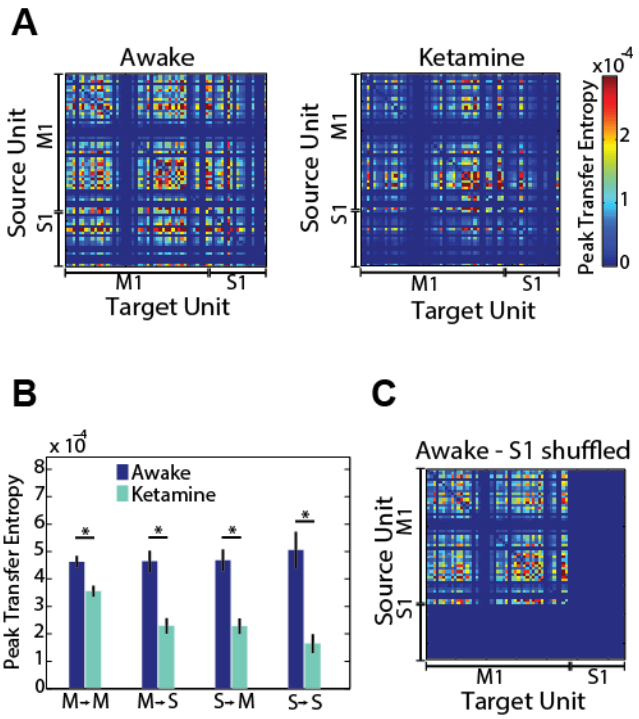

Figure 3.4 Loss of corticocortical effective connectivity under ketamine. (A) Peak high order transfer entropy (HOTE) between multiunit pairs during one monkey L experiment. (B) Comparison of Peak HOTE including all sessions for monkeys P and L. *p<.001. (C) HOTE between multiunit pairs after shuffling S1 spikes; same dataset as (A).

beyond task-relevant information transfer.

3.4.3. Spectral changes during ketamine exposure

Finally, we investigated changes in neural oscillations that could potentially explain the observed cortical disconnection. S1 exhibited changes in oscillatory activity that were time-locked with the administration of ketamine and correlated with the conscious state of the monkey (Fig. 3.5A-B). Relevant modulations in the delta (1-4 Hz), beta (15-30 Hz) and gamma (40-80 Hz) bands were observed in S1, while modulations in M1 beta and gamma were smaller, if at all present. The reversible decrease in beta and increase in delta and gamma power seen on S1 electrodes are directly homologous to our EEG observations in humans (Lee et al., 2013) during ketamine-induced unconsciousness, suggesting that the monkeys were in a comparable state of clinical anesthesia.

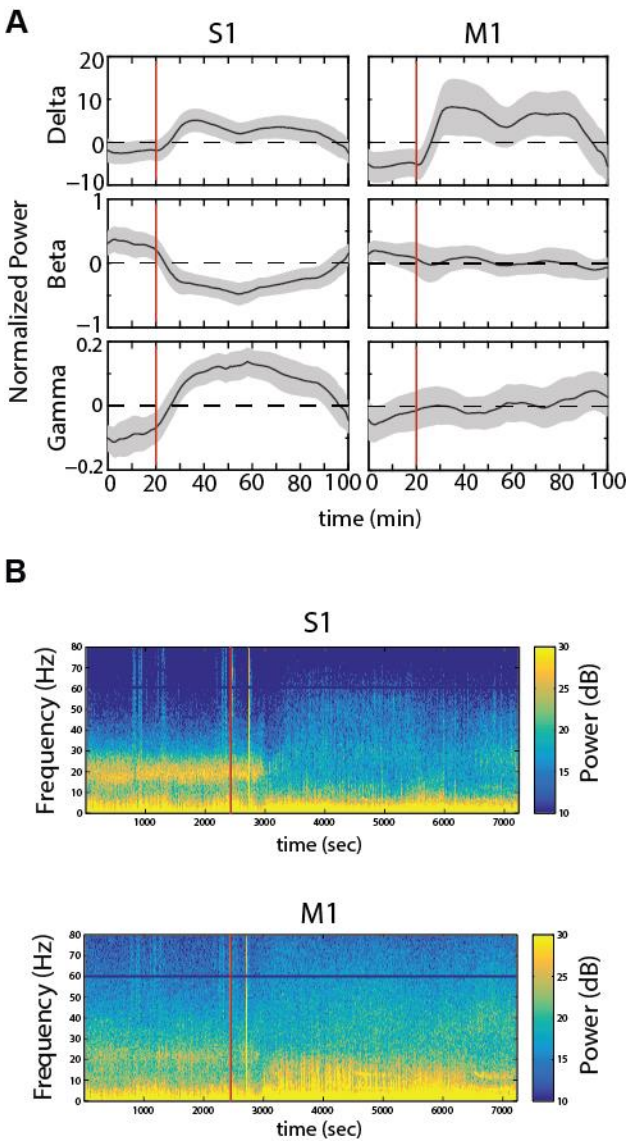

Figure 3.5 S1 electrodes lose beta power, gain gamma under ketamine. (A) Band power modulations of two monkey P sessions and two monkey L sessions (shaded area: SD, red vertical bar: injection). (B) Spectrograms from representative electrodes in S1 and M1 during a single Monkey L session (red vertical bar: injection).

3.5. Discussion

We have demonstrated that (1) primary sensory representation persists during ketamine anesthesia, as evidenced by the preserved ability to decode tactile stimuli in S1; (2) information transfer is disrupted between S1 and M1 during ketamine anesthesia, as evidenced by the inability to decode tactile stimuli in M1; (3) transfer

entropy, a surrogate for information exchange, is disrupted between neuronal units in S1 and M1; and (4) in S1, beta oscillations are suppressed while gamma and delta oscillations are augmented, as found with scalp EEG during ketamine anesthesia in humans. This experimental paradigm represents the most compelling evidence to date for reduced cortical information transfer and the unbinding of cortical representations in the anesthetized state (Mashour, 2013). One potential concern with this interpretation is the possibility that somatosensory information may be reaching M1 directly from thalamus, which would allow the possibility of a thalamocortical rather than a corticocortical breakdown of information exchange. According to the literature, the thalamus does not send M1 information about tactile sensation, only proprioception and other movement-related parameters (Rizzolatti and Luppino, 2001; Shipp, 2005). Regardless, the cortical connections between M1 and S1 are of primary interest here. Somatosensory stimulation is known to elicit both short- and long-latency evoked potentials in S1, with the long-latency responses attributed to corticocortical communication. It is these late responses that are normally associated with conscious awareness of a stimulus (Cauller and Kulics, 1991; Supèr et al., 2001; Del Cul et al., 2007) and selectively suppressed under anesthesia in S1 and primary visual cortex (V1) (Banoub et al., 2003; Hudetz et al., 2009). These late evoked responses are sometimes thought of as "top-down" processes, as they involve reentrant communication from areas higher in the cognitive hierarchy, such as association cortices. In the case of S1, motor areas are the source of some important top-down communication: Manita and colleagues (Manita et al., 2015) showed that long-latency inputs from M2 to S1 in the mouse were critical for accurate sensory perception. Taken together, the data support a top-down mechanism for accurate perceptual representation, where reciprocal corticocortical connections are necessary for conscious experience (Mashour, 2014).

Although disrupted cortical information transfer may represent a proximate cause for unconsciousness, the root cause of communication breakdown remains just as uncertain as the details of the communication itself. Top-down sensory processing necessitates coordination across distributed populations, a complex task that is almost certainly driven by oscillatory activity (Engel et al., 2001; Bressler and Richter, 2015). Low beta in particular, where we saw the most modulation, is relevant to top-down synchrony (Bressler and Richter, 2015), though we did not see significant modulations in M1. Beta oscillations have previously been implicated as information carriers in the sensorimotor system: synchronous beta activity in motor cortex

appears to mediate directionally-specific information flow (Rubino et al., 2006), and postcentral beta causally influences precentral beta (Brovelli et al., 2004). Conversely, gamma oscillations may mediate bottom-up, or feed-forward, sensory processing (Bressler and Richter, 2015), perhaps providing local gain on subsets of neurons (Pritchett et al., 2015). It is unclear whether our observed increase in gamma indicates an attempt at communication, or is simply the response of a circuit that has become disconnected and unbalanced. As for the origins of these waves, evidence supports the thalamus as responsible for overall control over cortical oscillations (Jones, 2001; Saalmann, 2014), and our data are consistent with the temporal binding model, where thalamocortical circuits synchronize cortical networks, modifying and enhancing cortical inputs to enable sensory awareness. Although the precise thalamic population responsible is unknown, ketamine is known to modulate normal thalamic function in general, as evidenced by increased glucose metabolism (Långsjö et al., 2005). Simultaneous cortical and thalamic recordings could potentially clarify these issues.

In summary, we have shown evidence for intact first-order thalamocortical information transfer to S1 during ketamine anesthesia and, through oscillatory behavior, indirect evidence for a higher-order thalamic influence on S1 that might account for the reduced transfer entropy of S1-M1 neuronal pairs that are functionally coupled in the waking state. The fact that this was demonstrated with the anesthetic ketamine is even more striking considering its unique traits at the molecular and systems neuroscience level. This direct demonstration of disrupted corticocortical information transfer, along with accumulating evidence for reduced surrogates of cortical communication during GABAergic anesthesia in humans (Ferrarelli et al., 2010; Casali et al., 2013; Lee et al., 2013), suggest a common final pathway for unconsciousness induced by molecularly distinct anesthetics. It should be noted, however, that spectral changes and depression of directed and effective connectivity can also be observed at subanesthetic doses of ketamine in humans (Lee et al., 2013; Muthukumaraswamy et al., 2015; Rivolta et al., 2015). Further work is required to assess whether functional disconnections in the cortex are epiphenomenal to general anesthesia or are dose-dependently reduced to a critical threshold that causes the anesthetized state.

Chapter 4

Individuated intracortical LEDs for optogenetic stimulation and interrogation of sensorimotor circuits

4.1. Abstract

Optogenetics studies in nonhuman primates currently take one of two approaches: inserting an optical fiber into cortex on a daily basis, causing damage and rendering long-term multichannel stimulation unfeasible, or stimulating and recording with a micro-electrocorticography grid, limiting the depth and placement of recordings. We wanted to develop an implant optimized for a primate study that allows for the arbitrary configuration of light sources as the experiment requires, including compatibility with intracortical microelectrode arrays. We wire bonded commercially available bare-die Cree blue LEDs (220x270x50 μm, 460nm wavelength) onto a glass wafer (100 μm thickness) and diced it to get individual devices. We used conductive epoxy to attach 75 μm wire to the devices, and dip coated them to provide strength and a watertight encapsulation. As a first step toward primate implants, we tested their functionality in a transgenic mouse model. We demonstrated their utility by performing a behavioral experiment, in which application of 50 Hz stimulation in motor cortex elicited robust increases in locomotion. We also demonstrated concurrent electrophysiological recordings by recording spikes from motor cortex while stimulating primary sensory cortex, a directly and densely connected region. These LEDs are novel compared with other devices in the literature in that they can be implanted individually in any configuration, including locations distant from recording sites, as well as surrounding an electrode array. The wires can run along the surface of the brain and emerge through the bone as a bundle, reducing strain and making the surgical close easier. Finally, they are fabricated simply, using commercially available materials.

4.2. Introduction

The current state of the art in light delivery in nonhuman primate (NHP) optogenetics is to use rigid glass optical fibers or microfabricated glass waveguides, either coupled to a recording electrode (Zhang et al., 2009; Abaya et al., 2012; Wang et al., 2012), or inserted separately (Jazayeri et al., 2012; Sparta et al., 2012; Ruiz et al., 2013). A high-power LED or laser is then coupled to the other end (Campagnola et al., 2008). In primates, this fiber must be inserted and removed for each recording session, limiting the number of total recording sessions based on tissue damage. It is possible to integrate fibers into a chronic Utah electrode array and let them remain in the brain for longer periods (Wang et al., 2012). Unfortunately, this has not been implemented successfully in primates without breaking the fibers or inflicting damage to the brain, due to motion of the brain inside the skull. An additional drawback of single-fiber implants in primates is the inability to excite or inhibit large volumes of brain. More recently, optogenetic stimulation and recording have been demonstrated in NHP using micro-electrocorticography (μECoG) grids (Yazdan-Shahmorad et al., 2015, 2016). Similar approaches have been taken *in vitro* (Poher et al., 2008; Grossman et al., 2010) and *in vivo* on the surface of the rodent cortex as part of an ECoG array (Ledochowitsch et al., 2011; Kwon et al., 2012). These are attractive, but it is unlikely light will penetrate deep enough into the primate brain to excite a large cortical volume. Light transmission through brain tissue falls off as one over the square of the distance to the source. Less than 1/8 of the original light will be transmitted at 1 mm away from the emitter (Aravanis et al., 2007), and we wish to excite cells 1.5 mm or more away from the surface. This is why optogenetic stimulation for brain-machine interfaces (BMI) seems to require intracortical devices.

In a recent paper, Kim et al. (2013) demonstrated the use of custom-made microLEDs for optogenetics. They injected their devices into rat cortex and were able to drive behavior in a place preference task. However, their devices were insulated with poly(dimethylsiloxane), or PDMS, which is not expected to retain a hermetic seal for many months (Lachhman et al., 2012). Montgomery et al. (2015) developed a wireless LED implant from commercially available LEDs with a parylene-C encapsulating coating. Both of these studies characterized the optical and thermal properties of their devices very well, but neither discussed device lifetime or showed

evoked action potentials, two very important features for many potential applications. Despite this, the success of the work in enabling behavioral experiments reinforces the notion that this is an outstanding problem in the field worth addressing. The prospect of putting powered electronics into the brain chronically has been daunting. If the insulation on implanted LEDs were to fail, the electrical power delivered directly to the tissue would be enough to cause damage. A conservative safe limit of leak current is 1 μA – this amount would not even stimulate the closest neuron to the device. Since our LEDs operate at 20 mA, it is essential to minimize the leakage current with hermetic encapsulation. Recording electrodes (like those in the Utah array (Hsu et al., 2009)) are typically insulated with parylene-C. Parylene has found widespread use due to its biocompatibility, high tensile strength, and relatively low water absorption. We also compared aramid nanofiber (ANF)/epoxy film, which has demonstrated superior adhesion performance than the more commonly used parylene-C in recent testing (Yang et al., 2011).

In this work, we created individually addressable intracortical devices that would be useful in a variety of rodent and NHP experiments, from basic neuroscience to patterned stimulation for brain-machine interfaces (BMIs). We demonstrated the capability of these devices to elicit motor behavior in mice, and to stimulate neurons in sensory cortex while simultaneously recording evoked action potentials with a recording electrode implanted in M1. We also performed accelerated lifetime soak testing of both parylene and aramid epoxy film coatings. The results of the soak testing indicate that safely packaging active electronics for long-term experiments remains a significant challenge and roadblock to chronic NHP implantation.

4.3. Methods

4.3.1. LED device fabrication

4.3.1.1. Mounting

Small (approximately 220um by 270um rectangular with 50um thickness) bare die LEDs are commercially available at the correct wavelengths and optical power for optogenetic stimulation. We chose Cree TR2227 devices for their minimal size, color, and power. The LEDs were wire bonded onto a 100 μm thick glass wafer patterned with gold pads, and diced to release individual devices with an ADT 7100 dicing saw (Advanced Dicing Technologies). Next, 75 μm copper wire (California Fine Wire, Grover Beach, California, #M287160) was attached by hand to the bond pads using conductive epoxy (EpoTek H20E), and oven cured. The optical output of the

devices were characterized with a Thorlabs power sensor (S302C, Thorlabs, Newton, New Jersey). Power density in mW/mm^2 was calculated by dividing by the area of the emitting surface of the die.

4.3.1.2. Hermetic coatings

We tested the performance of multiple coating materials: parylene-C, parylene-C with an additional aluminum oxide layer, and a medical grade epoxy.

For the epoxy devices, we used a layer by layer dip coating process incorporating aramid fibers. Macroscale aramid fiber, commonly known as Kevlar™, is a widely-used polymeric material for advanced composites. The unique advantages of aramid fibers include high tensile strength (~3.6 GPa), low density (~1.4g/cm3), and excellent thermal and chemical stability. Dispersions of aramid nanofibers (ANFs) with diameters ranging from 3 nm to 30 nm can be produced by dissolving bulk aramid fibers in organic solvent dimethyl sulfoxide (DMSO). When interlaid with medical grade epoxy, a clear, strong, and waterproof coating is formed. In this work, 1g of purchased Kevlar® thread was dissolved in 100ml of DMSO with 4g of KOH for a week to prepare a 10 mg/ml ANF dispersion. Each device was dipped into ANF nanofiber dispersion first, and then rinsed with water to remove the excess DMSO. Then, the device was dipped into 3% epoxy resin in acetone and dried at 80 degrees Celsius. This process was repeated until the device was covered in a 10 μm pinhole-free film.

For the parylene-C coatings, two groups of devices were prepared. The first group only received 10 μm parylene with silane adhesion promoter using a physical vapor deposition (PVD) process in a parylene deposition tool (Specialty Coating Systems). The second group subsequently received 52 nm of alumina (Al2O3) with an atomic layer disposition (ALD) tool (OpAL, Oxford Instruments) to enhance the hermeticity of the devices, as shown previously with Utah electrode arrays (Xie et al., 2014).

4.3.1.3. Driver circuitry

The voltages and currents applied to these devices need to be tightly regulated for safety purposes, and the timing of light pulses needs to be precise. We developed a custom shield for an Arduino Mega 2560 microcontroller board that can independently control 32 LEDs using two 16-channel LED drivers (TLC5940, Texas Instruments). A laptop running MATLAB was used

to communicate with the microcontroller via USB (Figure 4.1). The brightness of the LEDs was controlled with a digital potentiometer (AD5206, Analog Devices Inc.), and the generated pulses were synced with the neural data via a BNC hookup to the Arduino's digital output.

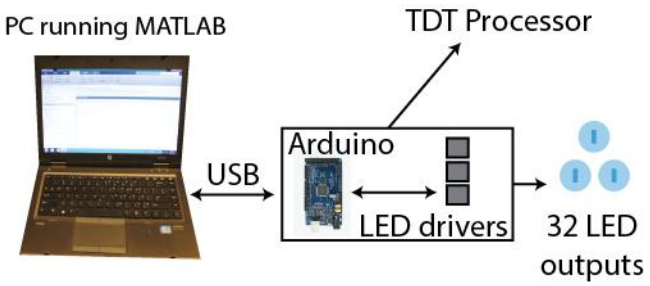

Figure 4.1 Control of optical stimulation. An Arduino microcontroller is used to drive the LEDs at the desired brightness, frequency, and duty cycle.

4.3.2. *In vivo* testing

All procedures and post-operative care complied with the University of Michigan's University Committee on Use and Care of Animals.

4.3.2.1. Surgery

Acute implantation of LEDs for demonstration of electrophysiological recordings was performed in two adult male Thy1-ChR2-YFP line 9 mice (Jackson Laboratories, stock no. 007615) weighing 26-28 g. Mice were first anesthetized using 4% isoflurane (v/v) to knock-out and then given an intraperitoneal (IP) injection of ketamine (100 mg/kg) with xylazine (10 mg/kg). Regular IP injections of ketamine (30 mg/kg) were given every 30 minutes to maintain anesthetic depth. Dual-shank tetrode probes (NeuroNexus, Ann Arbor, MI) deposited with PEDOT (as in Patel et al., 2015) to reduce site impedance were used for recordings. Reference and ground wires on the probe were attached to a single bone screw. Following craniotomies and resection of the dura, the probe was inserted into primary motor cortex (relative to bregma, AP:+1, ML:+1.5, DV:-.8 mm) with a digital stereotaxic frame. A single LED device was inserted into S1 (relative to bregma, AP:-0.9, ML:+3, DV:-1 mm). During surgery, animal vitals were monitored using a pulse-oximeter and rectal temperature probe.

Chronic implantation of LEDs for demonstration of induced behavior followed the same anesthesia protocol. Two mice (Thy1-ChR2-YFP line 18, Jackson Laboratories stock no. 007612) were each implanted with one LED device in M2 (relative to bregma, AP:+1, ML:+0.5,

DV:-1 mm). Dental acrylic was used to form a headcap, and a 2 pin header connector (Mill-Max, Oyster Bay, NY) was embedded in the acrylic for connecting the LED to power during experiments. The animals were recovered on a heating pad and were not optically stimulated until the following day.

4.3.2.2. Electrophysiology

The stimulator box (see 2.2) was used to stimulate neurons in S1 while recording from M1. Pulse trains were generated at 50 Hz (10% duty cycle, 2ms pulse width). All acquisition of electrophysiology recordings were taken using a ZC16 headstage, RA16PA pre-amplifier and RX5 Pentusa base station (Tucker-Davis Technologies, Alachua, FL). During data acquisition, the pre-amplifier high pass filtered at 2.2 Hz, anti-aliased filtered at 7.5 kHz, and sampled at a rate of ~25 kHz. Data from all working channels were common average referenced (CAR) to minimize stimulation artifact, imported into Offline Sorter (Plexon, Dallas, TX) and high-pass filtered (250 Hz corner, 4th order Butterworth). Each channel was manually thresholded and the sorted by a trained operator before exporting to MATLAB for plotting.

4.3.2.3. Behavioral experiment

The stimulator box (see 2.2) was used to stimulate neurons in M2 to elicit circling behavior. The two mice that were chronically implanted were each tested on the two days consecutively following their surgeries. They were placed in a clear behavioral chamber, and stimulated 10 times for 10 seconds each pulse train (50 Hz, 2 ms pulses), with 10 seconds of rest in between. Viewer software (Biobserve, St. Augustin, Germany) was used for motion tracking of the animal within overhead camera footage, and computed the percentage of time the animal was active (moving at least 0.1 cm/s).

4.3.3. Accelerated lifetime soak testing

A crucial aspect of this design is the hermetic seal of the LED packaging. In order to test the ability of this package to keep the LED dry for extended time in the brain, we performed accelerated soak tests of these devices in saline and use the Arrhenius equation to determine the mean-time-to-failure (Dokmeci et al., 1997; Harpster et al., 2005). Devices were soaked in 1x phosphate buffered saline (PBS) solution (BP3994, Fisher, Waltham, MA) in individual sealed vials (Figure 4.5A) in an incubator at 70ºC. Stimulus pulse trains and measurements were

performed with a PGSTAT12 Autolab (EcoChemie, Utrecht, Netherlands), controlled by vendor supplied NOVA software. On each day of measurements, the LEDs were removed from the incubator and pulsed at 50 Hz (10% duty cycle and 3 V pulse amplitude, the same parameters used in the *in vivo* experiments) for 10 minutes to simulate the stresses of an experiment. Then, one pulse was given below the turn-on voltage of the LED (1 V) while the current was measured, to approximate the leakage current. Finally, the 1 kHz impedance was measured. Measurements were taken every day for the first 7 days, and then every other day thereafter until failure. Failure occurred either by a lack of light output, a leakage current of greater than 1 μA, or a decrease in impedance of one order of magnitude or more, whichever occurred first.

4.4. Results

4.4.1. Fabrication

LED devices were created by wire bonding commercially available bare die LEDs onto a glass wafer, and dicing the wafer to release individuated LEDs (Fig. 4.2A). The glass serves two purposes. First, it provides bond pads that are large enough to interface with standard sized wire. Second, it slices through brain tissue easily to minimize the damage caused by insertion. Wires could then be attached (Fig. 4.2B) and the device treated with a waterproof coating (Fig. 4.2C).

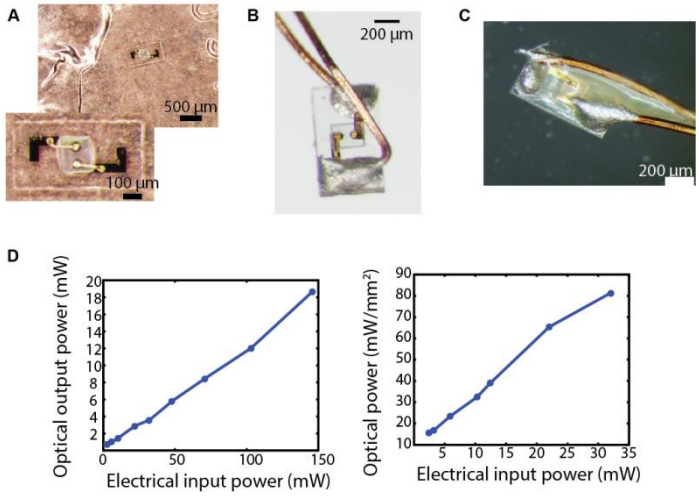

Figure 4.2 Device fabrication and characterization. (A) A single LED on glass after wire bonding and dicing. (B) A device after application of 75 μm wires. (C) A device after aramid nanofiber dip coating. (D) Optical power output of devices. The standard operating input power (20 mW) produces optical power density similar to that used with fiber-coupled lasers (50-60 mW/mm^2).

Using this process and very thin LEDs, we were able to keep the entire device under 500 µm thick. We believe this is an acceptable size to insert into the brain, being similar to many other neural probes and cannulae. The light output of the devices was measured to ensure sufficient light output following coating. We found that these devices could produce more than sufficient power (Fig. 4.2D). When operated at the recommended electrical input power, they emit similar optical power density to that used with fiber-coupled lasers (50-60 mW/mm^2).

4.4.2. *In vivo* testing

To demonstrate they can be used to drive behavior, aramid nanofiber coated LEDs were chronically implanted in area M2 (premotor cortex) of two mice. The devices were easily inserted into using a stereotaxic micromanipulator (Fig. 4.3A) without bleeding and with minimal dimpling of the cortex. We only implanted one device in each mouse, as they are significantly larger compared to the size of mouse brain than they would be in monkey, but no

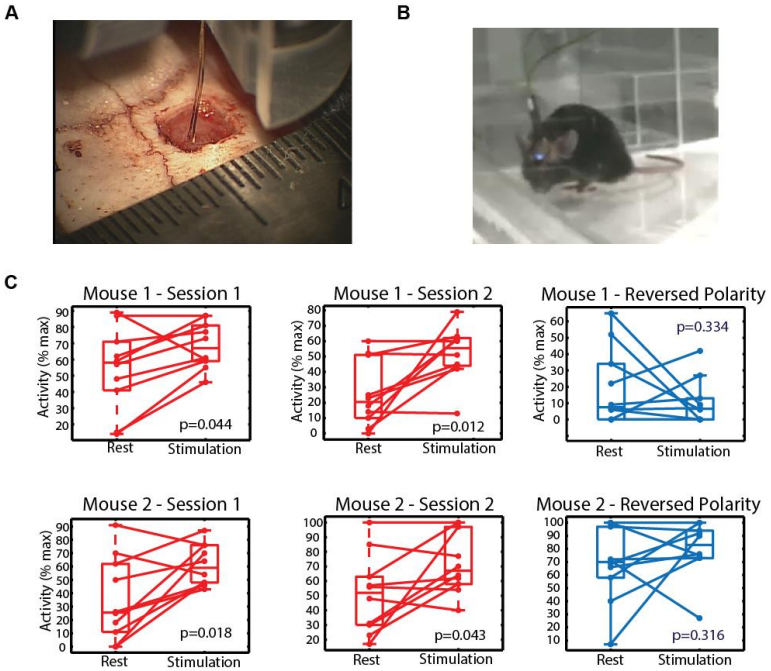

Figure 4.3 LEDs produce behavior in mice. (A) An LED device implanted 1 mm deep into mouse cortex, with wires visible. The device inserted with minimal dimpling and no bleeding. (B) Screen capture of mouse behavioral experiment. Blue light is visible through the acrylic headcap. (C) Behavioral data for two mice on two consecutive days. Mouse circling activity increased significantly (paired t-test) with 50 Hz stimulation (red), but not when LED was reverse biased (blue).

motor deficits were noted in the two chronically implanted animals. Stimulation of M2 at 50 Hz produced circling behavior in both mice (Fig. 4.3C) on two consecutive days. No effect was seen with reversed polarity stimulation, indicating that the observed behavior was not due to leakage current causing an electrical microstimulation (ICMS) effect.

To demonstrate the utility of these devices in electrophysiological experiments, we performed some acute recordings. Two separate mice were implanted with LED devices in primary somatosensory cortex (S1) and recording electrodes in primary motor cortex (M1) to mimic a BMI sensory feedback experiment (Fig. 4.4A). Spikes from multiple stimulus-responsive cells were recorded in each animal (Fig. 4.4B,C). While stimulus artifact was visible on many channels during recording, it could be mitigated with common average referencing (CAR), and was also easily separable during spike sorting. Perhaps due to the polysynaptic distance between

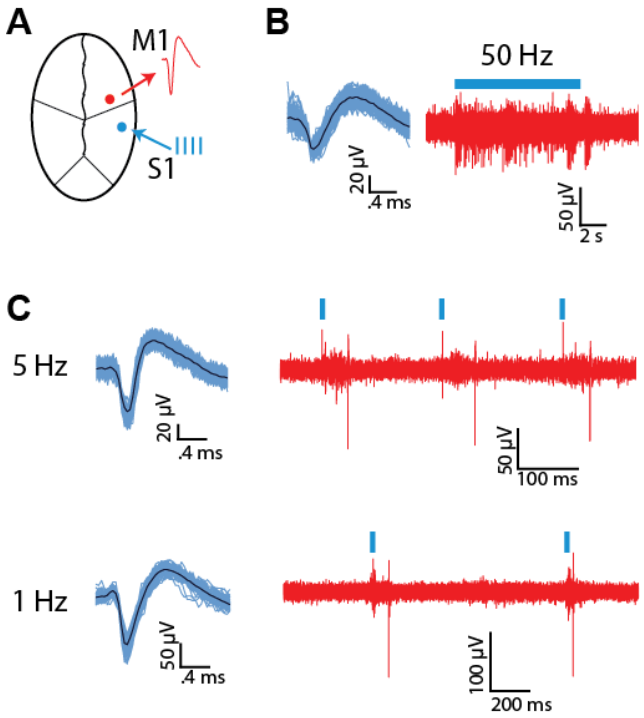

Figure 4.4 LEDs produce spikes in connected cortical regions. (A) Stimulation was delivered via LEDs implanted in S1, while recordings were taken from M1. (B) Example of M1 neuron that did not precisely follow a 50 Hz stimulus train (blue bar), but fired throughout the stimulus and exhibited onset and offset bursting. Left: all recorded waveforms of the given neuron with mean waveform overlaid. Right: spike trace after common average referencing. (C) Example M1 neurons that followed 5 Hz and 1 Hz stimulus trains. A small stimulus artifact is visible at time of LED pulses (blue strokes). Left: all recorded waveforms of the given neuron with mean waveform overlaid. Right: spike trace after common average referencing.

the stimulus and recording, cells did not precisely follow a 50 Hz stimulus train, but fired irregularly or in a bursting manner throughout. We observed multiple cells display a stimulus onset and offset bursting pattern (visible in the example cell in Fig. 4.4B). When the stimulus frequency was decreased, selected cells fired in a one-to-one manner following the stimulus train, with an expected interareal delay.

4.4.3. Longevity testing

Although these devices functioned well during short term mouse experiments, we needed to know how they would perform when implanted and stimulated through chronically, on the scale of weeks or months, before implanting in a monkey. The aramid epoxy coated devices in the chronically implanted mice stopped producing light after a few days of experiments, which led us to perform benchtop accelerated soak testing (Fig. 4.5A). We compared the performance of three coatings: aramid nanofiber epoxy, parylene, and parylene with alumina. The devices coated with parylene and alumina vastly outperformed the aramid epoxy and plain parylene coatings (Fig. 4.5C), though the majority of the devices were still failing at under one week of heated soaking, which is equivalent to six weeks at body temperature. This lifespan is sufficient for a rodent experiment, but most likely not for a chronic monkey implant. We investigated the cause of the coating failures by inspection under a microscope. No obvious holes or delamination in the coatings were found (Fig. 4.5B), implying that pinhole defects are likely the primary failure mode.

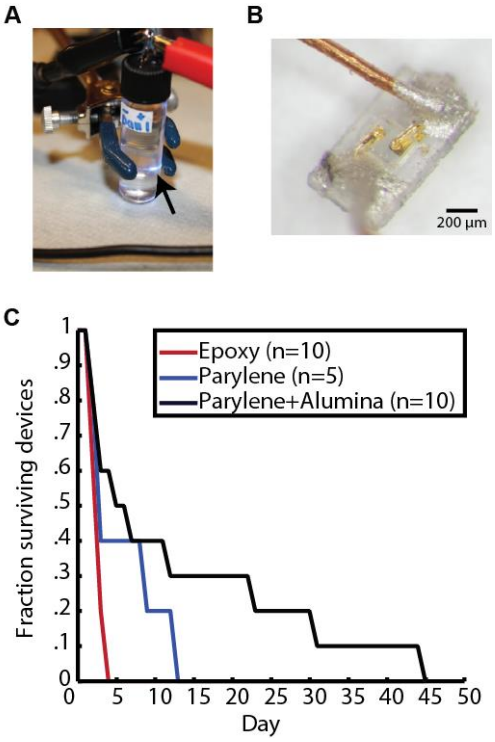

Figure 4.5 Soak testing of devices reveals longevity challenges. (A) LED soak testing vial with visible blue light (arrow). (B) Image of parylene and alumina coated device after failure. (C) Lifetimes of tested devices in heated saline soak with three different coatings.

4.5. Discussion

We fabricated implantable LEDs using inexpensive, off-the-shelf components, and relatively simple microfabrication processes. These devices produce enough light at the correct wavelength to excite neurons, and can be placed as desired to reach any cortical layer, or even subcortical structures.

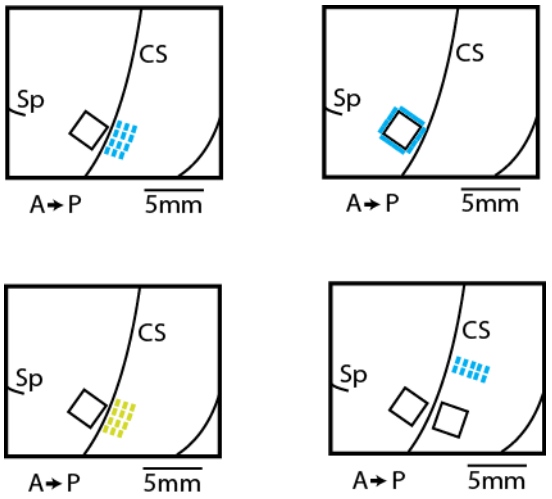

Figure 4.6 Examples of experiments that could be done in nonhuman primates with individuated optical stimulation devices. They include many-channel stimulation or inhibition (left top and bottom), illumination of entire Utah array recording volume (top right), and arbitrary placement of stimulation devices for sensory inputs (bottom right).

Given the results of accelerated soak testing, the LED implant described here (with parylene and alumina coating) is appropriate for both rodent experiments spanning multiple weeks and acute or short term primate studies. The longevity is somewhat limiting, but is explained by our rigorous stress testing. Most soak tests are performed passively, without actually passing current through the devices. We simulated 10 minutes of stimulation each day, which places a significant amount of stress on the coatings. Recent implantable LED papers (Kim et al., 2013; Montgomery et al., 2015) have not discussed longevity. These devices use similar coating materials, so we believe they likely suffer the same longevity challenges as those described here. The creation of a hermetic coating that is biocompatible, long-lasting under stressful conditions, thin, and optically clear remains an engineering challenge. Thicker coatings (beyond 10 µm) of the same materials tested here might extend device lifetime long enough to balance the tradeoff of a larger device. Complete glass encapsulation, or combined glass and silicon packaging, is another appealing option (Harpster et al., 2005).

Though challenges remain, we believe individuated implantable LEDs are a technology worth pursuing for their numerous applications in both primate and rodent work. Figure 4.6 shows several experimental configurations that could be done in a simple and cost-effective manner with these devices. Up to 32 independently addressable channels enable patterned stimulation for

sensory feedback in BMI experiments or for the study of communication between sensory and motor areas. Since the devices are not tied at all to the placement of recording electrodes, they can be moved to allow for more channels where they're needed. This also means they are compatible with Utah and other multielectrode arrays. The amount of photoelectric artifact on recording channels also decreases when the LEDs are moved farther away from the recording sites. This is an issue that is infrequently discussed in the literature, but rather mitigated by running LEDs on a DC voltage or sinusoidal stimulus rather than square pulses.

Future work will focus on the extension of device longevity and further miniaturization via refinement of the fabrication methods. Overall, the technology we fabricated and tested here represents a novel and useful approach to optogenetic stimulation of cortex, and could enable many circuit-level investigations where multiple input channels are desired.

Chapter 5

Discussion

> *"I felt what I was doing … it was exactly as it was my own fingers. What a feeling!"*
>
> -Upper limb prosthesis user describing his experience in a sensory feedback experiment. (Wijk and Carlsson, 2015)

5.1. Summary of work

In this thesis, we have presented further evidence for the importance of sensation to improved BMI performance, and detailed our progress in the development of technology to provide sensory feedback.

In the first study, we quantified the frequency and robustness of tactile somatosensory responses within the same M1 cortical populations that are used for motor decoding. We showed that some M1 neurons are naturally well tuned to tactile fingertip inputs, and that they can be tuned differently to different sensory modalities. These results highlight the importance of sensory information to motor control, even at the high level of the cortex. We know that control of movements without sensory feedback is difficult even with intact anatomy, in part because of natural variability in motor commands. There is now a body of evidence that the brain maintains accuracy by using a forward model that predicts the sensory consequences of motor commands (review, Shadmehr et al., 2010), which can then be updated via feedback (sensory prediction errors). The exact form of the model employed by M1 is not known, but Verstynen and Sabes (2011) developed an adaptive Bayesian model featuring Hebbian learning that mimicked the variance and directional biases of reaches made by humans. The presence of tactile representation in M1 implies that such computations are (at least in part) performed there. Of course, since human BMI are currently trained with visual observation or imagined movements,

and the only sensory stream available to M1 during task performance is visual, we would not expect to see the presence of tactile signals interfering with decodes. Instead, it is the *lack* of expected signal that the system is struggling to contend with. In monkey BMI, this same situation would be seen when monkeys are using brain control, and not allowed to touch the screen or manipulandum with the hand. However, in this case, the monkeys are usually trained on a manual task. Training the decoder in the presence of sensation and then expecting it to work properly once removing it is just as problematic. And once experimenters begin providing tactile feedback, e.g. with ICMS to S1, the presence of this signal will be something to contend with.

In the second study, we investigated the source of the tactile information, and its importance to sensory perception, using ketamine anesthesia. We showed that corticocortical communication of tactile information between S1 and M1 is interrupted during anesthetic-induced unconsciousness, while thalamocortical communication was maintained. As well as providing evidence for reduced cortical information transfer as a unifying property of anesthetic-induced unconsciousness, the data suggest that M1/S1 communication is necessary for accurate conscious perception of sensory inputs. This work further reinforces the need for sensory feedback in BMI experiments to enable naturalistic motor planning and execution.

In the final study, we presented the design and testing of intracortical optogenetic stimulation devices for the further exploration of sensory processing, as well as the delivery of sensory feedback in primate BMI experiments. We demonstrated that our implantable LED devices can safely drive behavior and neural activity in transgenic mice. When faced with hermetic encapsulation failure after a few days of use, we were spurred to perform accelerated soak testing of the devices using several candidate coating materials. We showed that a combination of parylene and aluminum oxide performed best, but with vast room for improvement. The ability to stimulate and record in different brain areas is a particularly useful achievement of this work, as this is precisely the setup that will be used for closed-loop BMI with tactile sensation.

5.2. Future directions

As we learn more about the extent to which sensory signals are essential to motor behavior, it is clear that we can no longer ignore this component of M1 activity if we want to continue to improve performance. It may seem as though we have created or uncovered more problems than

we have solved. Here, we suggest some avenues of research that we believe will advance our understanding of the system and move us toward high performance, closed-loop BMI systems.

5.2.1. Decoding

Decoders such as the Kalman filter (and even simpler linear estimation techniques) have achieved remarkable performance in highly constrained behavioral tasks such as cursor control and typing, even over several days without recalibration (Jarosiewicz et al., 2015). Calibrating the system in 'closed loop' mode certainly helps (Jarosiewicz et al., 2013). But what happens when we move into three dimensions, with prosthetics hands comprising many joints and real-world objects with strange dimensions that must be grasped and manipulated? As mentioned earlier, specialized calibration with objects is necessary before using decoders to interact with them (Wodlinger et al., 2015), and even with this training, there is room for improvement in performance. This is not surprising, as moving from two dimensional control to actually handling the weight and physics of an object is a large leap in complexity, both in the number of joints and muscles involved, and the mechanics of the environment. One solution is to use a state decoder to break the problem into more manageable pieces, then approach each piece (reach, grasp, lift, etc.) using its own unique model parameters based on separate training sessions. This has been executed successfully offline in monkeys performing a reach-to-grasp (Aggarwal et al., 2013), but it is unclear whether this approach will actually increase efficiency in online experiments.

Ultimately, decoding from linear models may not be the most promising approach. Instead of attempting to catalogue the contribution of each recorded neuron individually under every possible movement component, it may be better to take a step back and think about how the larger system initiates and executes a movement. Renewed interest in the dynamical systems perspective has led to some interesting findings; by reducing the dimensionality of a many-neuron data set, it's possible to observe the trajectory of the system through a state space that encompasses preparation and movement epochs (for review, see Shenoy et al., 2013). This approach employs the idea that there are many more neurons in M1 than muscles in the system it controls. Novel dimensionality reduction methods were developed that revealed a rotational structure to reaching trajectories (Churchland et al., 2012), suggesting non-periodic movements like reaches may be controlled in a similar way to rhythmic movements like walking, using a

central pattern generator. It has most recently been shown that reach kinematics are well represented in low-dimensional dynamics of M1 (as well as PMd and PMv) (Aghagolzadeh and Truccolo, 2016), and as some had predicted, decoding from these low-dimensional trajectories produced higher performance than decoding from the entire recorded neuronal population.

A large advantage of decoding based on trajectories extracted from M1 state space is its unsupervised nature. No assumptions are made about whether cells code for certain kinematics; rather, these associations fall out naturally. In this case, we can view sensory content of M1 firing rates as purely an asset to decoding. If modulation is strong enough, state space dimensions representing sensory responses or sensory processing will emerge as important. This technique has not been tested in the context of grasping and object manipulation, but it may be more suited to dealing with the rapidly changing cortical dynamics involved.

5.2.2. Stimulation

In Chapter 4, we discussed our success in developing implantable LEDs for cortical stimulation. We believe these devices will be useful for experiments exploring stimulation strategies for closed-loop control, but we are still faced with the problem of longevity. There are a few approaches to this problem. The first is to attempt thicker coatings; 10 μm parylene is commonly used in implanted devices, but this could easily be increased two or threefold in an attempt to extend device lifetime. If the primary failure mode is indeed pinholes or tiny cracks in the coatings, then a layer by layer process may help. The second is to find better coating materials. While the epoxy technology we tested did not outperform parylene, there are a few other options. One is to avoid films entirely and try a complete glass encapsulation, which could be achieved with by laser melting, or anodically bonded glass-silicon (Harpster et al., 2005). Graphene is another tempting possibility: it has recently been used to create transparent recording electrodes for simultaneous optical imaging (Kuzum et al., 2014), but could also be made as a nonconductive coating.

Once we have chronically implantable optical stimulation devices, we can ask a variety of interesting questions related to the timing and direction of sensory information flow between S1 and M1 and the response of M1 to various patterns of S1 stimulation while resting and during active movement. It has recently been demonstrated that monkeys can learn to interpret and use

multichannel ICMS in S1 representing proprioception to reach to nonvisible targets, and that they can integrate ICMS and visual feedback to achieve better performance on visible targets (Dadarlat et al., 2015). What has not yet been shown is how this stimulation affects M1 dynamics during an active motor task, a matter our devices would be well suited to addressing, since they enable simultaneous stimulation and recording. We can also investigate how much different types or amounts of stimulation can improve performance, and whether it is possible to put in multiple modalities of sensory information simultaneously.

Fortunately, there is ample evidence that cortex can learn to interpret new and somewhat arbitrary sensory inputs, and that M1 can adapt to non-ideal mappings. Sensorimotor learning in general involves learning new mappings between motor and sensory variables (Wolpert et al., 2011), whether those mappings represent the interactions between your fingers and some piano keys, or motor signals mapped directly from cortex with a BMI. Ganguly et al. (Ganguly and Carmena, 2009; Ganguly et al., 2011) demonstrated the creation of new cortical maps following perturbation of the way in which the decoder mapped firing rates to cursor control – tuning curves developed, deepened and then remained well-tuned for more than a week. They also showed that neurons not directly used in decoders underwent changes in tuning depth, though they were smaller than in directly used cells, and that multiple maps could be stored by the same population of cells, indicating widespread changes in motor cortical activity. Utilizing the idea that neuronal firing rates can be transformed into a low-dimensional subspace that captures important activity patterns, Sadtler et al. showed that monkeys could more easily adapt to perturbations within the original neural firing rate space, or "manifold" (Sadtler et al., 2014). Ideally, this will work out nicely in BMI control, as the point of stimulating in S1 is to allow M1 populations to behave as naturally as possible.

By continuing to work on these issues, it's very likely we will be able to develop a complete, clinically-viable BMI system that balances the risks of an invasive implantation surgery. The restoration of useful hand movement and sensation to those who have lost it stands to greatly improve the lives of those living with limb loss and paralysis.

BIBLIOGRAPHY

Abaya TVF, Blair S, Tathireddy P, Rieth L, Solzbacher F (2012) A 3D glass optrode array for optical neural stimulation. Biomed Opt Express 3:3087.

Aggarwal V, Acharya S, Tenore F, Shin HC, Etienne-Cummings R, Schieber MH, Thakor NV (2008) Asynchronous Decoding of Dexterous Finger Movements Using M1 Neurons. IEEE Trans Neural Syst Rehabil Eng 16:3–14.

Aggarwal V, Mollazadeh M, Davidson AG, Schieber MH, Thakor NV (2013) State-based decoding of hand and finger kinematics using neuronal ensemble and LFP activity during dexterous reach-to-grasp movements. J Neurophysiol 109:3067–3081.

Aggarwal V, Tenore F, Acharya S, Schieber MH, Thakor NV (2009) Cortical decoding of individual finger and wrist kinematics for an upper-limb neuroprosthesis. In: Annual International Conference of the IEEE Engineering in Medicine and Biology Society, 2009. EMBC 2009, pp 4535–4538.

Aghagolzadeh M, Truccolo W (2016) Inference and Decoding of Motor Cortex Low-Dimensional Dynamics via Latent State-Space Models. IEEE Trans Neural Syst Rehabil Eng 24:272–282.

Alkire MT, Hudetz AG, Tononi G (2008) Consciousness and Anesthesia. Science 322:876–880.

Amirikian B, Georgopulos AP (2000) Directional tuning profiles of motor cortical cells. Neurosci Res 36:73–79.

Andersen RA, Kellis S, Klaes C, Aflalo T (2014) Toward More Versatile and Intuitive Cortical Brain–Machine Interfaces. Curr Biol 24:R885–R897.

Antkowiak B (1999) Different actions of general anesthetics on the firing patterns of neocortical neurons mediated by the GABA(A) receptor. Anesthesiology 91:500–511.

Aravanis AM, Wang L-P, Zhang F, Meltzer LA, Mogri MZ, Schneider MB, Deisseroth K (2007) An optical neural interface: in vivo control of rodent motor cortex with integrated fiberoptic and optogenetic technology. J Neural Eng 4:S143–S156.

Asanuma DH, Larsen K, Yumiya H (1980) Peripheral input pathways to the monkey motor cortex. Exp Brain Res 38:349–355.

Banoub M, Tetzlaff JE, Schubert A (2003) Pharmacologic and physiologic influences affecting sensory evoked potentials: implications for perioperative monitoring. Anesthesiology 99:716–737.

Ben Hamed S, Schieber MH, Pouget A (2007) Decoding M1 neurons during multiple finger movements. J Neurophysiol 98:327–333.

Berg JA, Dammann, III JF, Tenore FV, Tabot GA, Boback JL, Manfredi LR, Peterson ML, Katyal KD, Johannes MS, Makhlin A, Wilcox R, Franklin RK, Vogelstein RJ, Hatsopoulos NG, Bensmaia SJ (2013) Behavioral Demonstration of a Somatosensory Neuroprosthesis. IEEE Trans Neural Syst Rehabil Eng 21:500–507.

Biddiss EA, Chau TT (2007) Upper limb prosthesis use and abandonment: A survey of the last 25 years. Prosthet Orthot Int 31:236–257.

Blain-Moraes S, Lee U, Ku S, Noh G, Mashour GA (2014) Electroencephalographic effects of ketamine on power, cross-frequency coupling, and connectivity in the alpha bandwidth. Front Syst Neurosci 8:114.

Boveroux P, Vanhaudenhuyse A, Bruno M-A, Noirhomme Q, Lauwick S, Luxen A, Degueldre C, Plenevaux A, Schnakers C, Phillips C, Brichant J-F, Bonhomme V, Maquet P, Greicius MD, Laureys S, Boly M (2010) Breakdown of within- and between-network resting state functional magnetic resonance imaging connectivity during propofol-induced loss of consciousness. Anesthesiology 113:1038–1053.

Boyden ES, Zhang F, Bamberg E, Nagel G, Deisseroth K (2005) Millisecond-timescale, genetically targeted optical control of neural activity. Nat Neurosci 8:1263–1268.

Bressler SL, Richter CG (2015) Interareal oscillatory synchronization in top-down neocortical processing. Curr Opin Neurobiol 31:62–66.

Brovelli A, Ding M, Ledberg A, Chen Y, Nakamura R, Bressler SL (2004) Beta oscillations in a large-scale sensorimotor cortical network: Directional influences revealed by Granger causality. Proc Natl Acad Sci U S A 101:9849–9854.

Campagnola L, Wang H, Zylka MJ (2008) Fiber-coupled light-emitting diode for localized photostimulation of neurons expressing channelrhodopsin-2. J Neurosci Methods 169:27–33.

Casali AG, Gosseries O, Rosanova M, Boly M, Sarasso S, Casali KR, Casarotto S, Bruno M-A, Laureys S, Tononi G, Massimini M (2013) A theoretically based index of consciousness independent of sensory processing and behavior. Sci Transl Med 5:198ra105.

Cauller LJ, Kulics AT (1991) The neural basis of the behaviorally relevant N1 component of the somatosensory-evoked potential in SI cortex of awake monkeys: evidence that backward cortical projections signal conscious touch sensation. Exp Brain Res 84:607–619.

Chestek CA, Gilja V, Blabe CH, Foster BL, Shenoy KV, Parvizi J, Henderson JM (2013) Hand posture classification using electrocorticography signals in the gamma band over human sensorimotor brain areas. J Neural Eng 10:026002.

Churchland MM, Cunningham JP, Kaufman MT, Foster JD, Nuyujukian P, Ryu SI, Shenoy KV (2012) Neural population dynamics during reaching. Nature 487:51–56.

Dadarlat MC, O'Doherty JE, Sabes PN (2015) A learning-based approach to artificial sensory feedback leads to optimal integration. Nat Neurosci 18:138–144.

Davidson J (2002) A survey of the satisfaction of upper limb amputees with their prostheses, their lifestyles, and their abilities. J Hand Ther 15:62–70.

Davidson JH, Khor KE, Jones LE (2010) A cross-sectional study of post-amputation pain in upper and lower limb amputees, experience of a tertiary referral amputee clinic. Disabil Rehabil 32:1855–1862.

Deisseroth K (2015) Optogenetics: 10 years of microbial opsins in neuroscience. Nat Neurosci 18:1213–1225.

Del Cul A, Baillet S, Dehaene S (2007) Brain Dynamics Underlying the Nonlinear Threshold for Access to Consciousness. PLoS Biol 5:e260.

Dokmeci MR, von Arx JA, Najafi K (1997) Accelerated testing of anodically bonded glass-silicon packages in salt water. In: , 1997 International Conference on Solid State Sensors and Actuators, 1997. TRANSDUCERS '97 Chicago, pp 283–286 vol.1.

Donoghue JP, Wise SP (1982) The motor cortex of the rat: cytoarchitecture and microstimulation mapping. J Comp Neurol 212:76–88.

Edin BB, Ascari L, Beccai L, Roccella S, Cabibihan J-J, Carrozza MC (2008) Bio-inspired sensorization of a biomechatronic robot hand for the grasp-and-lift task. Brain Res Bull 75:785–795.

Egan J, Baker J, House PA, Greger B (2012) Decoding Dexterous Finger Movements in a Neural Prosthesis Model Approaching Real-World Conditions. IEEE Trans Neural Syst Rehabil Eng 20:836–844.

Engel AK, Fries P, Singer W (2001) Dynamic predictions: oscillations and synchrony in top-down processing. Nat Rev Neurosci 2:704–716.

Ethier C, Oby ER, Bauman MJ, Miller LE (2012) Restoration of grasp following paralysis through brain-controlled stimulation of muscles. Nature 485:368–371.

Ferrarelli F, Massimini M, Sarasso S, Casali A, Riedner BA, Angelini G, Tononi G, Pearce RA (2010) Breakdown in cortical effective connectivity during midazolam-induced loss of consciousness. Proc Natl Acad Sci U S A 107:2681–2686.

Fetz EE, Finocchio DV, Baker MA, Soso MJ (1980) Sensory and motor responses of precentral cortex cells during comparable passive and active joint movements. J Neurophysiol 43:1070–1089.

Ganguly K, Carmena JM (2009) Emergence of a Stable Cortical Map for Neuroprosthetic Control. PLoS Biol 7:e1000153.

Georgopoulos AP, Schwartz AB, Kettner RE (1986) Neuronal population coding of movement direction. Science 233:1416–1419.

Gilja V, Nuyujukian P, Chestek CA, Cunningham JP, Yu BM, Fan JM, Churchland MM, Kaufman MT, Kao JC, Ryu SI, Shenoy KV (2012) A high-performance neural prosthesis enabled by control algorithm design. Nat Neurosci 15:1752–1757.

Grossman N, Poher V, Grubb MS, Kennedy GT, Nikolic K, McGovern B, Palmini RB, Gong Z, Drakakis EM, Neil MAA, Dawson MD, Burrone J, Degenaar P (2010) Multi-site optical excitation using ChR2 and micro-LED array. J Neural Eng 7:016004.

Harpster TJ, Nikles SA, Dokmeci MR, Najafi K (2005) Long-term hermeticity and biological performance of anodically bonded glass-silicon implantable packages. IEEE Trans Device Mater Reliab 5:458–466.

Harvey MA, Saal HP, Dammann JF, Bensmaia SJ (2013) Multiplexing Stimulus Information through Rate and Temporal Codes in Primate Somatosensory Cortex. PLoS Biol 11:e1001558.

Hatsopoulos NG, Suminski AJ (2011) Sensing with the Motor Cortex. Neuron 72:477–487.

Hochberg LR, Bacher D, Jarosiewicz B, Masse NY, Simeral JD, Vogel J, Haddadin S, Liu J, Cash SS, Smagt P van der, Donoghue JP (2012) Reach and grasp by people with tetraplegia using a neurally controlled robotic arm. Nature 485:372–375.

Hotson G, McMullen DP, Fifer MS, Johannes MS, Katyal KD, Para MP, Robert Armiger, Anderson WS, Thakor NV, Wester BA, Crone NE (2016) Individual finger control of a modular prosthetic limb using high-density electrocorticography in a human subject. J Neural Eng 13:026017.

Hsu J-M, Rieth L, Normann RA, Tathireddy P, Solzbacher F (2009) Encapsulation of an integrated neural interface device with Parylene C. IEEE Trans Biomed Eng 56:23–29.

Hudetz AG, Vizuete JA, Imas OA (2009) Desflurane Selectively Suppresses Long-latency Cortical Neuronal Response to Flash in the Rat. Anesthesiology 111:231–239.

Irwin Z, Thompson D, Schroeder K, Tat D, Hassani A, Bullard A, Woo S, Urbanchek M, Sachs A, Cederna P, Stacey W, Patil P, Chestek C (2015) Enabling Low-power, Multi-modal Neural Interfaces through a Common, Low-bandwidth Feature Space. IEEE Trans Neural Syst Rehabil Eng PP:1–1.

Ito S, Hansen ME, Heiland R, Lumsdaine A, Litke AM, Beggs JM (2011) Extending Transfer Entropy Improves Identification of Effective Connectivity in a Spiking Cortical Network Model. PLoS ONE 6:e27431.

Jarosiewicz B, Masse NY, Bacher D, Cash SS, Eskandar E, Friehs G, Donoghue JP, Hochberg LR (2013) Advantages of closed-loop calibration in intracortical brain–computer interfaces for people with tetraplegia. J Neural Eng 10:046012.

Jarosiewicz B, Sarma AA, Bacher D, Masse NY, Simeral JD, Sorice B, Oakley EM, Blabe C, Pandarinath C, Gilja V, Cash SS, Eskandar EN, Friehs G, Henderson JM, Shenoy KV, Donoghue JP, Hochberg LR (2015) Virtual typing by people with tetraplegia using a self-calibrating intracortical brain-computer interface. Sci Transl Med 7:313ra179.

Jazayeri M, Lindbloom-Brown Z, Horwitz GD (2012) Saccadic eye movements evoked by optogenetic activation of primate V1. Nat Neurosci 15:1368–1370.

Jones EG (2001) The thalamic matrix and thalamocortical synchrony. Trends Neurosci 24:595–601.

Jones EG, Coulter JD, Hendry SH (1978) Intracortical connectivity of architectonic fields in the somatic sensory, motor and parietal cortex of monkeys. J Comp Neurol 181:291–347.

Jones EG, Friedman DP (1982) Projection pattern of functional components of thalamic ventrobasal complex on monkey somatosensory cortex. J Neurophysiol 48:521–544.

Jones EG, Porter R (1980) What is area 3a? Brain Res Rev 2:1–43.

Kim S-P, Simeral JD, Hochberg LR, Donoghue JP, Black MJ (2008) Neural control of computer cursor velocity by decoding motor cortical spiking activity in humans with tetraplegia. J Neural Eng 5:455.

Kim T et al. (2013) Injectable, Cellular-Scale Optoelectronics with Applications for Wireless Optogenetics. Science 340:211–216.

Krubitzer L, Huffman KJ, Disbrow E, Recanzone G (2004) Organization of area 3a in macaque monkeys: Contributions to the cortical phenotype. J Comp Neurol 471:97–111.

Kuzum D, Takano H, Shim E, Reed JC, Juul H, Richardson AG, de Vries J, Bink H, Dichter MA, Lucas TH, Coulter DA, Cubukcu E, Litt B (2014) Transparent and flexible low noise graphene electrodes for simultaneous electrophysiology and neuroimaging. Nat Commun 5:5259.

Kwon KY, Sirowatka B, Li W, Weber A (2012) Opto- #x03BC;ECoG array: Transparent #x03BC;ECoG electrode array and integrated LEDs for optogenetics. In: 2012 IEEE Biomedical Circuits and Systems Conference (BioCAS), pp 164–167.

Lachhman S, Zorman CA, Ko WH (2012) Multi-layered poly-dimethylsiloxane as a non-hermetic packaging material for medical MEMS. In: 2012 Annual International Conference of the IEEE Engineering in Medicine and Biology Society (EMBC), pp 1655–1658.

Långsjö JW, Maksimow A, Salmi E, Kaisti K, Aalto S, Oikonen V, Hinkka S, Aantaa R, Sipilä H, Viljanen T, Parkkola R, Scheinin H (2005) S-ketamine anesthesia increases cerebral blood flow in excess of the metabolic needs in humans. Anesthesiology 103:258–268.

Ledochowitsch P, Olivero E, Blanche T, Maharbiz MM (2011) A transparent μECoG array for simultaneous recording and optogenetic stimulation. Conf Proc Annu Int Conf IEEE Eng Med Biol Soc IEEE Eng Med Biol Soc Conf 2011:2937–2940.

Lee U, Ku S, Noh G, Baek S, Choi B, Mashour GA (2013) Disruption of frontal-parietal communication by ketamine, propofol, and sevoflurane. Anesthesiology 118:1264–1275.

Lemon RN (1981) Functional properties of monkey motor cortex neurones receiving afferent input from the hand and fingers. J Physiol 311:497–519.

Lemon RN, Porter R (1976) Afferent Input to Movement-Related Precentral Neurones in Conscious Monkeys. Proc R Soc Lond B Biol Sci 194:313–339.

Lewis S, Russold MF, Dietl H, Kaniusas E (2012) User demands for sensory feedback in upper extremity prostheses. In: 2012 IEEE International Symposium on Medical Measurements and Applications Proceedings (MeMeA), pp 1–4.

Li Z (2014) Decoding methods for neural prostheses: where have we reached? Front Syst Neurosci 8 Available at: http://www.ncbi.nlm.nih.gov/pmc/articles/PMC4100531/ [Accessed April 29, 2016].

Lu J, Nelson LE, Franks N, Maze M, Chamberlin NL, Saper CB (2008) Role of endogenous sleep-wake and analgesic systems in anesthesia. J Comp Neurol 508:648–662.

Manita S, Suzuki T, Homma C, Matsumoto T, Odagawa M, Yamada K, Ota K, Matsubara C, Inutsuka A, Sato M, Ohkura M, Yamanaka A, Yanagawa Y, Nakai J, Hayashi Y, Larkum ME, Murayama M (2015) A Top-Down Cortical Circuit for Accurate Sensory Perception. Neuron 86:1304–1316.

Mashour GA (2013) Cognitive unbinding: A neuroscientific paradigm of general anesthesia and related states of unconsciousness. Neurosci Biobehav Rev 37:2751–2759.

Mashour GA (2014) Top-down mechanisms of anesthetic-induced unconsciousness. Front Syst Neurosci 8 Available at: http://www.ncbi.nlm.nih.gov/pmc/articles/PMC4066704/ [Accessed November 3, 2015].

Montgomery KL, Yeh AJ, Ho JS, Tsao V, Mohan Iyer S, Grosenick L, Ferenczi EA, Tanabe Y, Deisseroth K, Delp SL, Poon ASY (2015) Wirelessly powered, fully internal optogenetics for brain, spinal and peripheral circuits in mice. Nat Methods 12:969–974.

Morillon B, Hackett TA, Kajikawa Y, Schroeder CE (2015) Predictive motor control of sensory dynamics in auditory active sensing. Curr Opin Neurobiol 31:230–238.

Muthukumaraswamy SD, Shaw AD, Jackson LE, Hall J, Moran R, Saxena N (2015) Evidence that Subanesthetic Doses of Ketamine Cause Sustained Disruptions of NMDA and AMPA-Mediated Frontoparietal Connectivity in Humans. J Neurosci 35:11694–11706.

O'Doherty JE, Lebedev MA, Hanson TL, Fitzsimmons NA, Nicolelis MAL (2009) A brain-machine interface instructed by direct intracortical microstimulation. Front Integr Neurosci 3:20.

O"Doherty JE, Lebedev MA, Li Z, Nicolelis MAL (2012) Virtual Active Touch Using Randomly Patterned Intracortical Microstimulation. IEEE Trans Neural Syst Rehabil Eng 20:85–93.

Orsborn AL, Carmena JM (2013) Creating new functional circuits for action via brain-machine interfaces. Front Comput Neurosci 7 Available at: http://www.ncbi.nlm.nih.gov/pmc/articles/PMC3817362/ [Accessed March 16, 2016].

Patel PR, Na K, Zhang H, Kozai TDY, Kotov NA, Yoon E, Chestek CA (2015) Insertion of linear 8.4 μ m diameter 16 channel carbon fiber electrode arrays for single unit recordings. J Neural Eng 12:046009.

Pistohl T, Schulze-Bonhage A, Aertsen A, Mehring C, Ball T (2012) Decoding natural grasp types from human ECoG. NeuroImage 59:248–260.

Poher V, Grossman N, Kennedy GT, Nikolic K, Zhang HX, Gong Z, Drakakis EM, Gu E, Dawson MD, French PMW, Degenaar P, Neil MAA (2008) Micro-LED arrays: a tool for two-dimensional neuron stimulation. J Phys Appl Phys 41:094014.

Pritchett DL, Siegle JH, Deister CA, Moore CI (2015) For things needing your attention: the role of neocortical gamma in sensory perception. Curr Opin Neurobiol 31:254–263.

Qi H, Preuss T, Kaas J (2007) Somatosensory Areas of the Cerebral Cortex: Architectonic Characteristics and Modular Organization. In: The Senses: A Comprehensive Reference, Vol. 6 Somatosensation, pp 142–169. London: Elsevier.

Rivolta D, Heidegger T, Scheller B, Sauer A, Schaum M, Birkner K, Singer W, Wibral M, Uhlhaas PJ (2015) Ketamine Dysregulates the Amplitude and Connectivity of High-Frequency Oscillations in Cortical–Subcortical Networks in Humans: Evidence From Resting-State Magnetoencephalography-Recordings. Schizophr Bull 41:1105–1114.

Rizzolatti G, Luppino G (2001) The Cortical Motor System. Neuron 31:889–901.

Roberts L, Singhal G, Kaliki R (2011) Slip detection and grip adjustment using optical tracking in prosthetic hands. Conf Proc Annu Int Conf IEEE Eng Med Biol Soc IEEE Eng Med Biol Soc Conf 2011:2929–2932.

Rubino D, Robbins KA, Hatsopoulos NG (2006) Propagating waves mediate information transfer in the motor cortex. Nat Neurosci 9:1549–1557.

Ruiz O, Lustig BR, Nassi JJ, Cetin A, Reynolds JH, Albright TD, Callaway EM, Stoner GR, Roe AW (2013) Optogenetics through windows on the brain in the nonhuman primate. J Neurophysiol 110:1455–1467.

Saalmann YB (2014) Intralaminar and medial thalamic influence on cortical synchrony, information transmission and cognition. Front Syst Neurosci 8:83.

Saleem KS, Logothetis NK (2012) A Combined MRI and Histology Atlas of the Rhesus Monkey Brain in Stereotaxic Coordinates. Academic Press.

Salmi E, Långsjö JW, Aalto S, Någren K, Metsähonkala L, Kaisti KK, Korpi ER, Hietala J, Scheinin H (2005) Subanesthetic ketamine does not affect 11C-flumazenil binding in humans. Anesth Analg 101:722–725, table of contents.

Sanes JN, Donoghue JP (2000) Plasticity and Primary Motor Cortex. Annu Rev Neurosci 23:393–415.

Sanes JN, Schieber MH (2001) Orderly somatotopy in primary motor cortex: does it exist? NeuroImage 13:968–974.

Schieber MH (2001) Constraints on Somatotopic Organization in the Primary Motor Cortex. J Neurophysiol 86:2125–2143.

Schrouff J, Perlbarg V, Boly M, Marrelec G, Boveroux P, Vanhaudenhuyse A, Bruno M-A, Laureys S, Phillips C, Pélégrini-Issac M, Maquet P, Benali H (2011) Brain functional integration decreases during propofol-induced loss of consciousness. NeuroImage 57:198–205.

Shadmehr R, Smith MA, Krakauer JW (2010) Error Correction, Sensory Prediction, and Adaptation in Motor Control. Annu Rev Neurosci 33:89–108.

Shenoy KV, Sahani M, Churchland MM (2013) Cortical control of arm movements: A dynamical systems perspective. Annu Rev Neurosci 36:337–359.

Shipp S (2005) The importance of being agranular: a comparative account of visual and motor cortex. Philos Trans R Soc Lond B Biol Sci 360:797–814.

Simeral JD, Kim S-P, Black MJ, Donoghue JP, Hochberg LR (2011) Neural control of cursor trajectory and click by a human with tetraplegia 1000 days after implant of an intracortical microelectrode array. J Neural Eng 8:025027.

Sparta DR, Stamatakis AM, Phillips JL, Hovelsø N, Zessen R van, Stuber GD (2012) Construction of implantable optical fibers for long-term optogenetic manipulation of neural circuits. Nat Protoc 7:12–23.

Spinal Cord Injury and Paralysis Research Center (2009) Paralysis Facts & Figures. Available at: http://www.christopherreeve.org/site/c.mtKZKgMWKwG/b.5184189/k.5587/Paralysis_Facts__Figures.htm [Accessed June 14, 2013].

Suminski AJ, Tkach DC, Hatsopoulos NG (2009) Exploiting multiple sensory modalities in brain-machine interfaces. Neural Netw 22:1224–1234.

Supèr H, Spekreijse H, Lamme VAF (2001) Two distinct modes of sensory processing observed in monkey primary visual cortex (V1). Nat Neurosci 4:304–310.

Tanji J, Wise SP (1981) Submodality distribution in sensorimotor cortex of the unanesthetized monkey. J Neurophysiol 45:467–481.

Taylor DM, Tillery SIH, Schwartz AB (2002) Direct Cortical Control of 3D Neuroprosthetic Devices. Science 296:1829–1832.

Tennant KA, Adkins DL, Donlan NA, Asay AL, Thomas N, Kleim JA, Jones TA (2011) The organization of the forelimb representation of the C57BL/6 mouse motor cortex as defined by intracortical microstimulation and cytoarchitecture. Cereb Cortex N Y N 1991 21:865–876.

Velliste M, Perel S, Spalding MC, Whitford AS, Schwartz AB (2008) Cortical control of a prosthetic arm for self-feeding. Nature 453:1098–1101.

Verstynen T, Sabes PN (2011) How Each Movement Changes the Next: An Experimental and Theoretical Study of Fast Adaptive Priors in Reaching. J Neurosci 31:10050–10059.

Wang J, Ozden I, Diagne M, Wagner F, Borton D, Brush B, Agha N, Burwell R, Sheinberg D, Diester I, Deisseroth K, Nurmikko A (2011) Approaches to optical neuromodulation from rodents to non-human primates by integrated optoelectronic devices. In: 2011 Annual International Conference of the IEEE Engineering in Medicine and Biology Society,EMBC, pp 7525–7528.

Wang J, Wagner F, Borton DA, Zhang J, Ozden I, Burwell RD, Nurmikko AV, van Wagenen R, Diester I, Deisseroth K (2012) Integrated device for combined optical neuromodulation and electrical recording for chronic in vivo applications. J Neural Eng 9:016001.

Wijk U, Carlsson I (2015) Forearm amputees' views of prosthesis use and sensory feedback. J Hand Ther 28:269–278.

Wodlinger B, Downey JE, Tyler-Kabara EC, Schwartz AB, Boninger ML, Collinger JL (2015) Ten-dimensional anthropomorphic arm control in a human brain−machine interface: difficulties, solutions, and limitations. J Neural Eng 12:016011.

Wong YC, Kwan HC, MacKay WA, Murphy JT (1978) Spatial organization of precentral cortex in awake primates. I. Somatosensory inputs. J Neurophysiol 41:1107–1119.

Wu W, Gao Y, Bienenstock E, Donoghue JP, Black MJ (2006) Bayesian Population Decoding of Motor Cortical Activity Using a Kalman Filter. Neural Comput 18:80–118.

Xie X, Rieth L, Williams L, Negi S, Bhandari R, Caldwell R, Rohit Sharma, Tathireddy P, Solzbacher F (2014) Long-term reliability of Al 2 O 3 and Parylene C bilayer encapsulated Utah electrode array based neural interfaces for chronic implantation. J Neural Eng 11:026016.

Yang M, Cao K, Sui L, Qi Y, Zhu J, Waas A, Arruda EM, Kieffer J, Thouless MD, Kotov NA (2011) Dispersions of Aramid Nanofibers: A New Nanoscale Building Block. ACS Nano 5:6945–6954.

Yazdan-Shahmorad A, Diaz-Botia C, Hanson T, Ledochowitsch P, Maharabiz MM, Sabes PN (2015) Demonstration of a setup for chronic optogenetic stimulation and recording across cortical areas in non-human primates. In, pp 93052K – 93052K – 6 Available at: http://dx.doi.org/10.1117/12.2080405 [Accessed April 13, 2016].

Yazdan-Shahmorad A, Diaz-Botia C, Hanson TL, Kharazia V, Ledochowitsch P, Maharbiz MM, Sabes PN (2016) A Large-Scale Interface for Optogenetic Stimulation and Recording in Nonhuman Primates. Neuron 89:927–939.

Zagha E, Casale AE, Sachdev RNS, McGinley MJ, McCormick DA (2013) Motor Cortex Feedback Influences Sensory Processing by Modulating Network State. Neuron 79:567–578.

Zhang F, Aravanis AM, Adamantidis A, Lecea L de, Deisseroth K (2007) Circuit-breakers: optical technologies for probing neural signals and systems. Nat Rev Neurosci 8:577–581.

Zhang J, Laiwalla F, Kim JA, Urabe H, Van Wagenen R, Song Y-K, Connors BW, Zhang F, Deisseroth K, Nurmikko AV (2009) Integrated device for optical stimulation and spatiotemporal electrical recording of neural activity in light-sensitized brain tissue. J Neural Eng 6:055007.

Zhang Y, Chen Y, Bressler SL, Ding M (2008) Response preparation and inhibition: the role of the cortical sensorimotor beta rhythm. Neuroscience 156:238–246.

Ziegler-Graham K, MacKenzie EJ, Ephraim PL, Travison TG, Brookmeyer R (2008) Estimating the Prevalence of Limb Loss in the United States: 2005 to 2050. Arch Phys Med Rehabil 89:422–429.